Fusion Engineering and Design 85 (2010) 243–265

Contents lists available at ScienceDirect

Fusion Engineering and Design

journal homepage: www.elsevier.com/locate/fusengdes

An advanced computational algorithm for systems analysis of tokamak power plants

Zoran Dragojlovic[a,*], A. Rene Raffray[a], Farrokh Najmabadi[a], Charles Kessel[b], Lester Waganer[c], Laila El-Guebaly[d], Leslie Bromberg[e]

[a] University of California in San Diego, La Jolla, CA, United States
[b] Princeton Plasma Physics Laboratory, Princeton, NJ, United States
[c] Boeing Consultant, St. Louis, MO, United States
[d] Fusion Technology Institute, University of Wisconsin, Madison, WI, United States
[e] Plasma Fusion Center, Massachusetts Institute of Technology, Cambridge, MA, United States

ARTICLE INFO

Article history:
Received 8 July 2009
Received in revised form 31 January 2010
Accepted 9 February 2010
Available online 12 March 2010

Keywords:
ARIES
Systems code
Economic analysis
Cost of electricity
Fusion power plants

ABSTRACT

A new computational algorithm for tokamak power plant system analysis is being developed for the ARIES project. The objective of this algorithm is to explore the most influential parameters in the physical, technological and economic trade space related to the developmental transition from experimental facilities to viable commercial power plants. This endeavor is being pursued as a new approach to tokamak systems studies, which examines an expansive, multi-dimensional trade space as opposed to traditional sensitivity analyses about a baseline design point. The new ARIES systems code consists of adaptable modules which are built from a custom-made software toolbox using object-oriented programming. The physics module captures the current tokamak physics knowledge database including modeling of the most-current proposed burning plasma experiment design (FIRE). The engineering model accurately reflects the intent and design detail of the power core elements including accurate and adjustable 3D tokamak geometry and complete modeling of all the power core and ancillary systems. Existing physics and engineering models reflect both near-term as well as advanced technology solutions that have higher performance potential. To fully assess the impact of the range of physics and engineering implementations, the plant cost accounts have been revised to reflect a more functional cost structure, supported by an updated set of costing algorithms for the direct, indirect, and financial cost accounts. All of these features have been validated against the existing ARIES-AT baseline case. The present results demonstrate visualization techniques that provide an insight into trade space assessment of attractive steady-state tokamaks for commercial use.

1. Introduction

The Advanced Reactor Innovation and Evaluation Study (ARIES) [1] is a national, multi-institutional research program, which performs progressive, integrated design studies of the long-term fusion energy devices for general consumer utilities. The goal of this activity is to identify key research and development (R&D) directions and to provide visions for the US fusion program. An important route towards this goal is through systems studies of advanced fusion power plant concepts. A traditional approach to fusion power plant systems analysis is to design the optimal power plant and explore the sensitivity of this design to local perturbations in the most critical parameters [2]. This approach was exercised through all the past ARIES design studies, including the most recent steady state tokamak reactor ARIES-AT [3]. Traditionally, the ARIES systems code was utilized [4–7] within the ARIES project as a tool for parametric search of a design point [8] that yields the lowest cost of electricity for the prescribed constraints and operational parameters. However, the search for a single optimal point is not sufficient to provide an insight into a vast multi-dimensional space of possibly attractive "near-optimal" designs and may have a difficulty justifying the selection of that particular point.

Recently, the ARIES team has focused on identifying the R&D needs in transition from experimental tokamak facilities, such as ITER, to fully operational power plants (i.e., Demo and beyond). In this case, tradeoffs over wide regions of physics and engineering design parameters are sought. In order to fulfill this objective, a new systems code is being developed as a computational tool that integrates the state-of-the-art physics, engineering, and costing algorithms. The new structure of the systems code is modular

* Corresponding author at: 1800 South Maple Street, Apartment 214, Escondido, CA 92025, United States. Tel.: +1 760 233 1341.
E-mail addresses: zoran@fusion.ucsd.edu, zdragojlovic@gmail.com (Z. Dragojlovic).

0920-3796/$ – see front matter © 2010 Elsevier B.V. All rights reserved.
doi:10.1016/j.fusengdes.2010.02.015

and composed from a custom-made toolbox of generic, easy-to-assemble building blocks. The steady state plasma physics for advanced tokamaks is modeled by an algorithm that was already developed in order to examine the high field compact tokamak burning plasmas for the fusion ignition research experiment (FIRE) [9]. The reactor model includes the radial build, nuclear parameters, power core and energy conversion systems that are compatible to the ARIES-AT [10] but can easily be altered from this design. For example, the current tokamak model has an option of implementing different blanket concepts, such as the advanced $Pb - 17Li + SiC_f/SiC$ concept and the dual coolant $Pb - 17Li + FS + He$ concept, in order to assess the impact of blanket design on the technological and economic attractiveness of the power plant. The former blanket option was used with the ARIES-AT with liquid Pb–17Li as breeder and coolant. The latter option, also known as dual coolant lithium lead (DCLL) blanket, was developed using helium in the first wall in order to mitigate the MHD-induced pressure drop due to the circulation of high velocity liquid metal to cool the first wall (FW) in the presence of a magnetic field. The proposed solution was to use helium as a coolant for the FW and structural box and a lower velocity self-cooled Pb–17Li as a breeder. Both blanket concepts were analytically evaluated on a compact stellarator ARIES-CS [11] and their comparison revealed some economic penalties associated with the DCLL concept [11,12]. Those penalties include a thicker blanket and higher pumping costs due to the introduction of helium, as well as decreased passive safety rating, resulting in higher level of safety assurance. As a consequence, the total cost of the DCLL blanket was higher [12] for the compact stellarator, but no similar comparison exists for tokamaks at present.

The new tokamak model has a magnetic confinement system that resembles the one used for the ARIES-AT in geometry, while updated algorithms were used for the material composition, size and cost of two magnet options: low temperature superconducting magnet (~4.2 K) and high temperature superconducting magnet (~75 K).

The structural support of the toroidal field (TF) magnet is estimated by scaling from the finite element analysis reported in Ref. [13]. The breakdown of all the fusion power plant costing accounts was originally suggested by Schulte et al. [14], who introduced the direct and indirect cost accounts and defined some of the algorithms that are presently used. A complete and well-documented cost assessment was given by Waganer et al. [15] in the STARFIRE conceptual power plant study. The GENEROMAK report [16] developed a basis for a parametric reactor design with modeling algorithms based largely on STARFIRE [15]. The ESECOM study [17] was the first to employ safety assurance credit factors for use with design concepts employing advanced fuels or low activation materials to reduce capital costs on specific systems and subsytems. This credit concept evolved into the Level of Safety Assurance as first employed in ARIES-II, IV final report [18]. The costing accounts and the associated algorithms have been further updated through the 1990s–2000s ARIES design concepts, such as ARIES-I, II, IV, RS, SPPS, ST, and AT. A thorough revision of this costing breakdown is currently in progress in order to reflect a more functional cost structure.

The ARIES systems algorithm is outlined and compared to its predecessor code in Section 2. The plasma physics module of the code is described in Section 3. A detailed overview of the power core is given in Section 4, where special attention is paid to the radial build, magnetic confinement system and blanket options. The power flow is described in Section 5, with a detailed description of two power cycles associated with different blanket options. Filtering of tokamak power plants through different engineering criteria is outlined in Section 6. Costing algorithms are overviewed in Section 7, with a detailed account of all the components that comprise the cost of electricity. Example results that highlight the utility of the systems code are demonstrated in Section 8, followed by a discussion and guidelines for future development, given in Section.

2. ARIES systems code

2.1. Motivation and overall plan

During the past 20 years, the ARIES team has developed several advanced magnetic fusion concepts, including tokamaks (ARIES-I, ARIES-II&IV, ARIES-RS, ARIES-AT and Pulsar), the ARIES-ST spherical torus, the TITAN reversed-field pinch, and stellarators (SPPS and ARIES-CS). All of these concepts are derived from systems studies integrated with detailed off-line physics and engineering analyses, which utilized the most advanced known methods at the time. This approach will be retained in the future. However, several major deficiencies of the previous systems code will be addressed, such as outdated engineering and costing models, lack of modularity, difficulty of upgrading to new features and limited approach to finding the optimal operating point.

The new ARIES systems code is being written in order to generate an updated, more accurate model of an advanced, steady state D-T fuelled tokamak. In addition to building the new algorithms, a new computational strategy is being devised in order to accommodate the change of focus from analyzing a single data point to investigating a wide, multi-dimensional operational design space. The new objective is to identify tradeoffs in operating parameters that will lead to highly desirable tokamak solutions that might lessen or eliminate major constraints. The new systems code has a number of advantages compared to the former algorithm:

- All the modules of the new code are generated from a custom-made, general purpose toolbox, which is built to allow an easy way to assemble an arbitrary, but viable tokamak model.
- In order to efficiently generate a large database of tokamak solutions, physics and engineering filters are implemented at early stages of calculation to eliminate any non-valid design points.
- A new physics module derived from the proposed FIRE design study implements the most current knowledge in simulating advanced steady state plasmas.
- Engineering algorithms provide a complete update of the power core elements with 3D geometry and a more realistic power flow.
- Costing algorithms are updated in order to reflect the latest costing methodology.
- 2D and 3D visualization techniques are developed and utilized in order to provide an insight into parametric design space of advanced tokamaks.

2.2. Algorithm layout

The ARIES systems code consists of three distinctive modules, which are physics, engineering and costing, as shown in Fig. 1. The physics module generates a large set of viable operating plasmas for advanced, high fusion performance tokamaks. The engineering module creates the inboard, outboard and top/bottom radial builds for the blanket, divertor, shield, vacuum vessel and TF coils, a power extraction and conversion system for given plasma, 3D power core configuration, and the power flow model from nuclear fusion power to net electric power. The costing module estimates the direct and indirect capital cost of the entire plant including more detailed costs for the power core. These capital costs are converted to annualized costs and added to the annual costs for operations and maintenance, fuel, scheduled component replacement, and decommissioning to determine the cost of electricity. The cost of electricity is the figure of merit and the final output of the systems code.

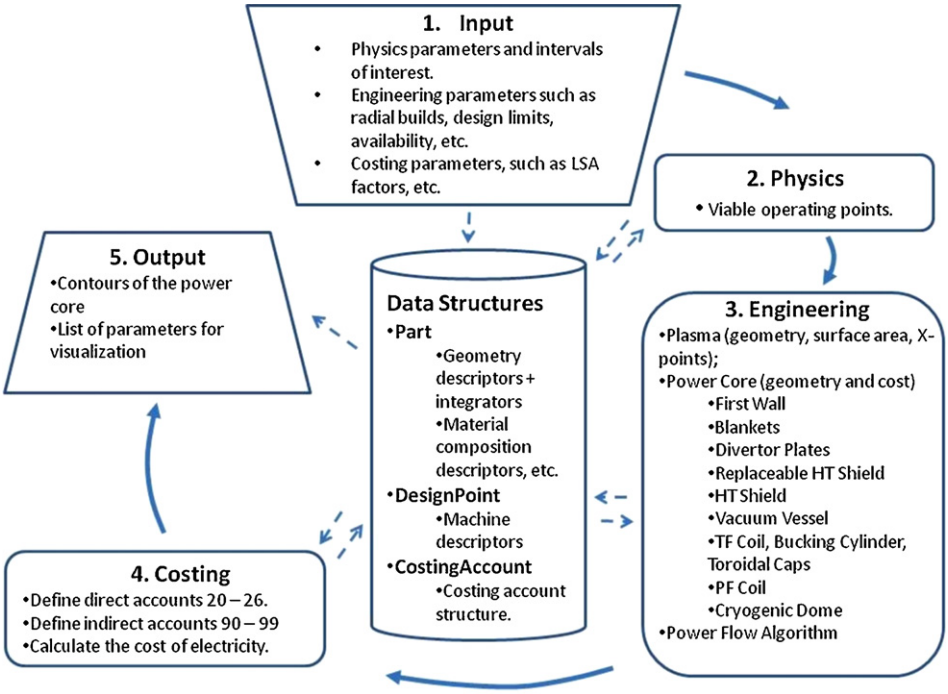

Fig. 1. Flow chart of the ARIES systems algorithm.

The foundation of the algorithm is a general purpose systems analysis toolbox. This toolbox consists of ready-to-use generic C++ classes, which serve as building blocks for the power plant model. Class "*DesignPoint*" holds design-specific data that describe the entire machine, including plasma and nuclear parameters, power core builds, power flow, etc. These data are accessed, operated on and displayed by special functions that belong to the same class. Class "*Part*" holds part-specific data which describe the geometry, thickness, composition, material properties and unit costs of the individual components of the fusion reactor. This class also holds higher level properties that are derived from part-specific data such as volume, cross-sectional area and total cost. Simple declaration statement such as "*Part BlanketDCLL*" declares all the variables and associated functions needed to define a power core object, in this case for the dual coolant lithium-lead and helium blanket. Class "*CostingAccount*" contains the costing account structure for a D-T-fueled tokamak. A model of the power plant is generated by building the power core from pre-defined components, setting all the desired machine properties and functions within the *DesignPoint* object, defining the *CostingAccount* structure and connecting all these elements together in order to estimate the cost of electricity.

2.3. Inputs and outputs

The input parameters to the ARIES systems code are given in Tables 1–5. Table 1 shows the names of the inputs to the plasma physics algorithm. The rationale for choosing the values of these parameters is discussed in Section 3. The input variables to the engineering algorithms consist of the power core inboard, outboard and divertor radial builds with corresponding material compositions (Table 2), magnetic confinement system inputs (Table 3), and power flow inputs (Table 4). The inputs to the costing algorithm are given in Table 5. The numerical values provided here are based on earlier studies or recommendations, as referenced in Tables 1–5.

The output from the new ARIES systems code consists of 3D contours of the power core elements, which are provided in order to depict and analyze the geometry of the tokamak model and physics/engineering/costing data for systems analysis. The latter group of data parameters are graphically presented via custom-designed 2D and 3D parametric plots, which are designed in order to enhance the diagnostics and provide insight into the parametric design space based on the large number of data points.

3. Plasma physics

The 0D analysis is provided by the plasma module that solves the global plasma power balance and particle balance using a series of models and established physics relationships, typically for fixed plasma geometry (R, a, and shape). Parabolic equations with pedestal profile prescriptions for plasma density and temperature are used:

$$n(r) = (n_0 - n_a)\left[1 - \left(\frac{r}{a}\right)^2\right]^{\alpha_n} + n_a \tag{1}$$

The pedestal value is applied at the plasma edge, not at what is typically considered the pedestal location in experimental devices. For the density profile $n_a/n(0)$ is given and for the temperature profile $T_a/T(0)$ is given. These values are chosen to provide a reasonable match to profiles obtained in 1.5-D analysis. The exponent is varied to provide the desired peak-to-volume average. The plasma power and particle balance can be described by

$$\frac{dW}{dt} = 0 = P_\alpha + P_{aux} + P_{ohmic} - P_{brem} - P_{cycl} - fP_{line} - \frac{W}{\tau_E} \tag{2}$$

$$\frac{dn_{He}}{dt} = 0 = \frac{n_{DT^2}\langle\sigma\upsilon\rangle}{4} - \frac{n_{He}}{\tau^*_{He}} \tag{3}$$

which includes quasi-neutrality, $n_e = n_{DT} + 2n_{He} + \sum Z_j n_j$. The factor f on the line radiation term is explained below. The ratio of τ^*_{He}/τ_E is prescribed and provides the link between the power and particle balance equations. The alpha power is provided by the Bosch–Hale formulation [20], the auxiliary power is inputed or determined to provide some other constraint. The fusion power and line radiation terms are calculated on fictitious flux surfaces and integrated due to their profile sensitivities. The ohmic,

Table 1
Physics input parameters for the ARIES systems code.

Parameter	Symbol	Parameter	Symbol
1. Toroidal magnetic field at plasma major radius.	B_T	14. Internal self-inductance.	a_{li}
2. Plasma aspect ratio.	A	15. Ejima coefficient, used to calculate internal self-consumption.	c_e
3. Normalized toroidal beta.	β_n	16. V-s required in breakdown phase of discharge.	$f_{\text{breakdown}}$
4. Cylindrical safety factor (q_{cyl} if +, q_{95} if −).	q_{cyl} q_{95}	17. Current drive efficiency for source i, $i = 0, 1, 2, 3, 4$.	η^i_{CD}
5. Plasma triangularity.	δ	18. Input current drive power for source i, $i = 1, 2, 3, 4$.	P^i_{CD}
6. Exponent on density profile.	a_n	19. Radial location for source i, $i = 1, 2, 3, 4$.	r^i_{CD}
7. Exponent on temperature profile.	a_t	20. Plasma major radius.	R
8. Greenwald density fraction.	f_{Gw}	21. Starting and final value of confinement multiplier used in search for power balance.	$h_{\min}$, $h_{\max}$
9. Fusion gain.	Q	22. Additional value of plasma elongation to use in transport equation.	a_{kx}
10. Plasma elongation.	κ	23. Charge of impurity j, $j = 1, 2, 3$.	z^j_{imp}
11. Input flattop time.	t_{flati}	24. Fraction of electron density of impurity j, $j = 1, 2, 3$.	f^j_{imp}
12. V-s available.	d_{fcs}	25. Ratio of plasma edge temperature to central temperature.	t_{rat}
13. Confinement time ratio ($t_{\text{global particle}}/t_{\text{energy}}$).	t_{pote}	26. Ratio of plasma edge density to central density.	d_{rat}

Table 2
Builds and material composition.

Builds [19]	
Inboard radial build for elements i, including scrape-off layer, first wall, inboard blanket, shield, vacuum vessel, and cryogenic dome.	δ_i
Variation of inboard shield thickness with NWL:	
$\delta_{shield,inb} = c_{inb} + 6.7 \cdot \ln(NWL/3.3)$	
Outboard radial build for elements j, including scrape-off layer, first wall, blanket I, blanket II, shield, and vacuum vessel.	δ_j
Variation of outboard shield thickness with NWL:	
$\delta_{shield,outb} = c_{outb} + 6.64 \cdot \ln(NWL/3.3)$	
Divertor build for elements k, including divertor plates, divertor shield, and vacuum vessel.	δ_k
Variation of top/bottom shield thickness with NWL:	
$\delta_{shield,t/b} = c_{t/b} + 6.64 \cdot \ln(NWL/3.3)$	
Material composition [19]	
Material name for material n, $n = 1, \ldots, N$, where N is the total number of materials.	$MAT(n)$
Density [kg/m^3]	$\rho(n)$
Volume fraction [–]	$f_V(n)$
Density fraction [–]	$f_\rho(n)$
Cost per unit mass (unit cost) [$/kg]	$c(n)$
Unit cost year [–]	$Y_c(n)$

Table 3
Inputs to magnet algorithms.

Parameter	Symbol/Value	Parameter	Symbol/Value
TF magnet inputs			
1. Maximum stress in protective sheath around strands.	$\sigma_{sheath} = 800\,\text{MPa}$	6. Current density in Cu.	$J_{Cu} = 224\,\text{MA/m}^2$
2. Current density in the superconductor.	$J_{SC} = f(B_T^{\max})$	7. Side thickness of the coil casing.	$b = 2\,\text{cm}$
3. Volume fraction of the He coolant.	f_{He}	8. Maximum magnetic field in the TF coil.	$B_T^{\max} = 18\,\text{T}$
4. Volume fraction of the insulator.	f_{ins}	9. Nominal current in TF coil.	$I_{TF} = 40\,\text{kA}$
5. Maximum allowed stress in the coil casing.	$\sigma_b = 400\,\text{MPa}$	10. Number of TF coils.	$N = 16$
PF magnet inputs			
1. Maximum allowed stress in PF coil.	$\sigma = 760\,\text{MPa}$	5. Current limiters.	$q_{\max} = 4.5$ $q_{\min} = 3.15$
2. Rate of change of coil current with flux state.	$\frac{\partial c}{\partial p}$	6. Maximum stress in sheath.	$\sigma_{sheath} = 800\,\text{MPa}$
3. Maximum magnetic field in PF coils.	$B_{PF}^{\max} = 18\,\text{T}$	7. Quench protection parameters for Cu.	$J_{2\tau} = 5 \times 10^{16}\,\frac{A^2 s}{m^4}$ $\tau = 2\,\text{s}$
4. Coil currents at zero flux state.	c^1_{coil} c^2_{coil}	8. Total number of PF coils.	$N_{PF} = 36$

Table 4
Power flow inputs.

Parameter	Symbol/Value	Parameter	Symbol/Value
Power conversion factors			
1. Fraction of loss of alpha particles.	$f_{\alpha\,loss} = 0$	5. Symmetry factor.	$f_{sym} = 1$
2. Fraction of alpha loss to divertor.	$f_{\alpha\,div} = 0.5$	6. Outboard-inboard split of the absorbed power.	$f_{ncf}^{outboard} = 0.6$ $f_{ncf}^{inboard} = 0.4$
3. Fraction of radiation to divertor.	$f_{div\,rad} = 0.75 - 0.90$	7. Split of power between FW/blanket and shield fraction.	$f_{FW/blanket} = 0.9$ $f_{shield} = 0.1$
4. Fraction of edge radiation.	$f_{rad\,edge} = 0.9$	8. Split of neutron power between divertor plates, divertor blanket and divertor shield.	$f_{div\,plates} = 0.5$ $f_{div\,shield} = 0.5$
Neutron energy multiplication factors			
1. First wall/blanket.	$f_{FW/blanket}^{mul\,inb}$ $f_{FW/blanket}^{mul\,outb}$	3. Divertor plates, divertor blanket and divertor shield.	$f_{divertor}^{mul}$ $f_{blanket}^{mul}$ f_{shield}^{mul}
2. Shield.	$f_{shield}^{mul\,inb}$ $f_{shield}^{mul\,outb}$		
Peaking factors and limits			
1. Neutron wall load peaking factor [30].	$nwl_{peak} = f(A)$	2. Maximum heat flux to divertor.	$q_{div}^{max} = 5 \div 22\,MW/m^2$
Efficiencies			
1. Coolant pump efficiency.	η_{pump}	3. Current drive power source efficiencies (a generic term η_{CD}^{gen} can be used as a less accurate alternative).	$\eta_{CD}^{NB} = 0.68$ $\eta_{CD}^{LH} = 0.68$ $\eta_{CD}^{ICRF} = 0.84$ $\eta_{CD}^{EC} = 0.43$ $\eta_{CD}^{gen} = 0.5$
2. Efficiency of conversion from thermal to gross electric power.	$\eta_{power\,cycle}$ (typically Brayton or Rankine)		
Powers			
1. Power for auxiliary functions.	$P_{aux\,func} = 50\,MW$	2. Cryogenic power.	$P_{cryo}^{Nb_3Sn} = 2\,MW$ $P_{cryo}^{HTS} = 0.5\,MW$
3. He pumping power.	$P_{pump,He}$		

bremsstrahlung, and line terms are given, respectively, by

$$P_{ohm} = (1 - f_{bs})(0.5/l_i)\eta_{neo} I_p^2/\pi^2 a^4 \kappa^2 \quad (4)$$

$$P_{brem} = 5.3 \times 10^{-37} Z_{eff} n_e^2 \sqrt{T_e} \quad (5)$$

$$P_{line} = n_e \sum n_z L_z \quad (6)$$

where coronal equilibrium has been assumed and the Post–Jensen [21] data are used. Up to 3 impurities, in addition to He, can be specified. The ohmic formulation is approximate, but has been shown to agree well with TSC simulations. The resistivity is the neoclassical formulation evaluated using volume average temperature, inverse aspect ratio at half radius, and a fixed collisionality of 0.05. The cyclotron term is taken from Albajar [22–24] which represents a significant improvement over the old Trubnikov [25] treatment. The wall reflection must be specified, and is only approximate since this quantity is very complicated to determine. The bootstrap current and current drive power are evaluated using the following equations:

$$\begin{aligned} a_1 &= 1.10 - 1.165 l_i + 0.47 l_i^2 \\ b_1 &= 0.806 - 0.885 l_i + 0.297 l_i^2 \\ C_{bs} &= a_1 + b_1 \frac{n(0)}{\langle n \rangle} \\ f_{bs} &= C_{bs} \sqrt{\varepsilon} \beta_p \end{aligned} \quad (7)$$

Table 5
Inputs to costing accounts.

Parameter	Symbol/Value	Parameter	Symbol/Value
1. Cost base year for the output costs.	Y_{base}	6. Worth of revenue requirements for unit investment that is deprecated for tax purposes over 5 years.	$F = 1.272$
2. Level of safety assurance.	$LSA = 1$ for SiC system $= 2$ for FS system	7. Contingency cost factor.	$f_{96} = 0.195$
3. Cost credit factors.	$f_{cc}(LSA)$	8. Annual escalation rate.	$y = 0.05$
4. Effective tax-adjusted cost of money (discount rate).	$X_0 = 0.0435 \frac{\$}{year}$	9. Construction period.	$Y = 6\,years$
5. FW end-of-life fluence.	$l_{nf}^{SiC} = 18 \frac{MWyear}{m^2}$ $l_{nf}^{DCLL} = 15 \frac{MWyear}{m^2}$	10. Plant capacity factor.	$p_f = 0.85$

$$P_{CD} = \frac{n_e R I_p (1 - f_{bs})}{\eta_{CD}} \tag{8}$$

which is a fit to a large number of equilibrium calculations, and where the current drive efficiency η_{CD} is prescribed. The energy confinement time is provided by a scaling relationship in terms of the global plasma parameters. The most recent scaling adopted for ITER is the IPB98(y,2) [26] expression given by

$$\tau_E^{IPB(y,2)} = 0.1445 H_{98}(y,2) M^{0.19} I_p^{0.93} R^{1.97} B_T^{0.15} \varepsilon^{0.58} \kappa_a^{0.78} \overline{n_{e20}}^{0.41} / P_{loss}^{0.69} \tag{9}$$

where the factor $H_{98}(y, 2)$ provides a method for making the global confinement time higher or lower than the scaling. The elongation is evaluated at the plasma separatrix, but is defined as the plasma cross-section area divided by πa^2. The loss power is defined as

$$P_{loss} = P_\alpha + P_{ohmic} + P_{aux} - P_{brem} - P_{cycl} - P_{line}/3 \tag{10}$$

where the reduction of the line radiation is intended to account for the fact that the majority of line radiation is emitted from the plasma edge which does not directly affect the core plasma power balance where fusion is taking place. This is confirmed by 1.5-D simulations. It should be noted that the line radiation term reduction must be applied consistently everywhere, in the power balance and the expression for global energy confinement time. The power threshold for L to H transition is given by the scaling relationship [27]:

$$P_{LH} = 2.84 B_T^{0.82} \overline{n_{e20}}^{0.58} R^{1.0} a^{0.81} / M \tag{11}$$

or [28]

$$P_{LH} = 0.042 n_{20}^{0.73} B_T^{0.74} S^{0.98} \tag{12}$$

and the power to be compared to this threshold is the loss power noted above with the line radiation reduction. Both of the scaling relationships for the global energy confinement time and the LH threshold were determined from present tokamak experiments ignoring radiation. However, in the application to power plants, radiation is included since it represents a significant loss mechanism from the core plasma that is not present in experimental devices. There are other L to H threshold expressions available and these expressions can be used, if desired.

When the specific heating and current drive (H&CD) systems are specified, based on more detailed analysis outside the systems code, up to four different types of H&CD systems can be specified, each with their own deposition location and CD efficiency. Some examples might be the following,

$$\begin{aligned} I_{FW} &= \eta_{FW} P_{FW} / n(r/a = 0) R \\ I_{NBI} &= \eta_{NBI} P_{NBI} / n(r/a = 0.25) R \\ I_{LH} &= \eta_{LH} P_{LH} / n(r/a = 0.75) R \\ I_{EC} &= \eta_{EC} P_{EC} / n(r/a = 0.4) R \end{aligned} \tag{13}$$

where I, P and η are the current, power and efficiency of the current drive, respectively. The subscripts *FW*, *NBI*, *LH*, and *EC* denote the types of the current drive typically used in tokamaks, such as "fast wave", "neutral beam injection", "lower hybrid" and "electron cyclotron", respectively. The relationships depicted in Eq. (13) could be enhanced with specific Z_{eff} dependencies.

Several physics relationships are used in the 0D calculations and these are listed below.

$$\begin{aligned} n_{Gr} &= I_p / \pi a^2 \\ \beta &= \beta_N I_p / a B_T = 2\mu_0 \langle p \rangle_\upsilon / B_T^2 \\ q_{95} &= (\pi a^2 B_T / \mu_0 R I_p) \frac{(1 + \kappa^2 (1 + 2\delta^2 - 1.2\delta^3))}{(1 - \varepsilon^2)^2} (1.17 - 0.65\varepsilon) \\ q_{cyl} &= \pi a^2 B_T (1 + \kappa^2) / \mu_0 R I_p \\ V &= 2\pi R \pi a^2 \kappa \\ \beta_p &= 12.5 \beta_N B_T a (1 + \kappa^2) / I_p \end{aligned} \tag{14}$$

3.1. Calculating a physics operating space

In order to establish a database of viable physics operating points, any of the input variables can be scanned over a range. The names of the input parameters for the systems code physics module are shown in Table 1. One can specify four specific heating and current drive sources in terms of deposition location, CD efficiency, input power, or fraction of plasma current to be driven. An example of a scan might be the following

$$\begin{aligned} B_T &= 5.0 - 10.0T \\ \beta_N &= 0.03 - 0.06 \\ q_{95} &= 3.2 - 4.0 \\ \frac{n}{n_{Gr}} &= 0.4 - 1.0 \\ Q &= 25 - 50 \\ \tau_{He}^*/\tau_E &= 5 - 10 \\ R &= 4.8 - 7.8m \end{aligned} \tag{15}$$

with all other parameters fixed at specific values. Once a database is established, a series of physics filters are applied to eliminate some unphysical solutions that can arise from the physics equations. These filters are

$$\begin{aligned} P_{CD} &\le P_{heat} \\ f_{bs} &\le 1.0 \\ \tau_{He}^*/\tau_E &> 4.0 \end{aligned} \tag{16}$$

Once the filtering is complete any additional filters can be further applied to eliminate unfeasible or not attractive engineering solutions or to examine specific parameter ranges of the physics operating space. The physics module creates a database file which is read by the engineering module.

The output of the physics module of the systems code contains the parameters listed in Table 6.

4. Power core

A typical cross-section of the tokamak power core generated by the systems code is shown in Fig. 2. The plasma contour is defined by the limiting flux surface. The contours of all the objects depicted are represented by the sequence of 2nd order polynomials, which can be integrated to obtain volumes and cross-sections as needed. The number and spacing of the defining points along each contour are adjustable in order to resolve any geometrical detail required. Material cost of the power core elements is taken into account by the volume and density fractions of the components, their densities and unit costs. The details of this operation are described in Section 4.2, on the example of the TF coil. Fig. 2 is a 2D representation of the solids revolved about the power core center line. Volume fractions are used to account for non-solid elements. Discrete elements in the toroidal direction, like the TF coils are handled as an area

Table 6
Output from physics module of ARIES systems code.

Parameter	Symbol	Parameter	Symbol
1. Plasma current.	I_p	19. Flattop time.	$t_{flattop}$
2. Toroidal beta.	β_t	20. Global energy confinement time.	τ_E
3. Poloidal beta.	β_p	21. Global effective particle confinement time.	τ_P
4. Normalized beta.	β_n	22. Current profile resistive diffusion time.	τ_J
5. Alpha power.	P_α	23. Bootstrap current fraction	f_{BS}
6. Bremsstrahlung radiated power.	P_{brem}	24. Average neutron wall load at plasma surface.	NWL
7. Cyclotron radiated power.	P_{cycl}	25. Helium fraction in plasma relative to electrons.	f_{He}
8. Line radiation.	P_{line}	26. Total DT fuel density fraction relative to electrons.	f_{DT}
9. L to H mode threshold power.	P_{LH}	27. Fast particle beta from alphas.	β_{fast}
10. Ratio of loss power to L to H threshold power.	$\frac{P_{loss}}{P_{LH}}$	28. Global energy confinement time scaling factor.	$H_{98(y,2)}$
11. Fusion power.	P_{fusion}	29. Thermal stored energy in plasma.	W_{th}
12. Heating power required for plasma power balance.	P_{aux}	30. Total consumed V-s.	$\Delta\psi_{cons}$
13. Ohmic power.	P_{ohm}	31. Flattop loop voltage.	V_{loop}
14. Volume average density.	$\langle n_e \rangle$	32. Fraction of plasma current from external CD sources.	f_{CD}
15. Density weighted volume average temperature.	$\langle T_e \rangle$	33. Total non-inductive current fraction, bootstrap + external CD.	f_{NI}
16. Ratio of flattop time to current profile resistive diffusion time.	$\frac{t_{flattop}}{\tau_J}$	34. Peak-to-volume average density.	$\frac{n(0)}{\langle n \rangle}$
17. Total radiated power fraction.	f_{rad}	35. Peak-to-volume average temperature.	$\frac{T(0)}{\langle T \rangle}$
18. Effective charge.	Z_{eff}		

times the toroidal thickness. The main body of the vacuum vessel is shown in Fig. 2, but there is significant volume in the maintenance ports between individual TF coils. The divertors are not shown in sufficient detail for definition in this figure.

4.1. Radial build and nuclear parameters

The nuclear assessment defines the radial builds and provides an essential set of nuclear parameters for the systems code. This parameter set includes the tritium-breeding ratio (TBR), neutron energy multiplication (Mn), nuclear heat load to all the components, poloidal distribution of neutron wall loadings (NWL), radiation damage to structural components and their service lifetimes. A calculated TBR of 1.1 assures tritium self-sufficiency for all ARIES designs with Pb–17Li breeder [29]. All the components, such as blanket, shield, manifolds, and vacuum vessel of past ARIES designs [30,19,31,11] provided a combined shielding function. With guidance from the thermo-mechanical analysis, the nuclear analysis defines the first wall and blanket parameters, which include thickness, composition, and ^{6}Li enrichment. Besides breeding sufficient amounts of tritium for plasma operation/permeation/decay and recovering more than 90% of the neutron energy, the first wall/blanket assembly protects the shield for the entire plant life not to exceed 200 dpa, projected as 40 full-power years (FPY). Additionally, the shield is designed to protect the welds of the manifolds and vacuum vessel (such that they should not exceed 1 He appm). The vacuum vessel composition and dimensions are optimized to essentially protect the superconducting magnets and maintain the radiation level below the limits specified by the magnet designers. All the ARIES materials should be carefully chosen to enhance the shielding performance and minimize the long-term environmental impact. All the components should be sized for the maximum NWLs on the inboard (IB), outboard (OB), and divertor with adequate performance margins compared to requirements. The first wall/blanket and divertor system along with a few shielding components are replaceable, designed to have identical service lifetimes, while the external power core subsystems are designed with a 40 FPY lifetime. Typical nuclear parameters for the DCLL and PbLi/SiC blankets are summarized in Table 7.

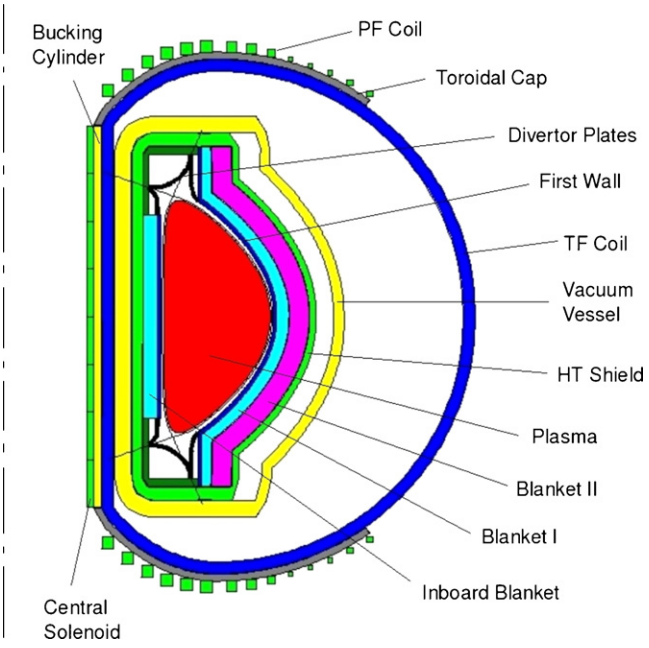

Fig. 2. Cross-section of the power core segment generated by the ARIES systems code.

4.2. Magnets

Costs of magnetic plasma confinement have a high impact on the cost of electricity, therefore toroidal and poloidal field magnets

Table 7
Key nuclear parameters for the DCLL and LiPb/SiC systems.

Blanket concept	LiPb/He/FS	LiPb/SiC
Calculated overall TBR	1.1	1.1
^{6}Li enrichment	$\leq$ 90%	$\leq$ 90%
FW end-of-life fluence [MWyear/m^2]	15	18
FW/blanket lifetime (FPY)	$\simeq$3	$\simeq$4
Shield/manifold/VV/magnet lifetime (FPY)	40	40
Overall energy multiplication	1.15	1.1

are modeled as accurately as the scope of the systems code allows. In general, the definition and total cost of a magnet is obtained by executing the following steps. More detail on each step will follow.

1. Retrieve the costing data for the magnet components from the *Part* class. These data include mass densities, costs per unit mass and cost base years.
2. Retrieve the relevant magnetic or structural data for the magnet components.
3. Estimate the cross-sectional area of each component so that the current density and/or stress remain within the acceptable limits. Assuming a known variation of thickness along the perimeter of the magnet coil, this information translates into volume fractions of the magnet components.
4. Generate the 3D contours of the magnet.
5. Integrate across the magnet contours to obtain the total volume of the magnet and its components.
6. Calculate the cost of each component and sum up the costs.

The assumed materials and the corresponding algorithms used for the initial analysis are outlined in the following sub-sections. It is planned to add other possible superconducting and structural materials in future versions of the code to provide a more complete database for larger parametric studies.

4.2.1. Toroidal field magnet algorithm

The toroidal field (TF) magnet consists of 16 coils of a constant width, with a shape composed from two semi elliptic profiles that are joined at the vertical axis, as shown in Fig. 3. A portion of the inner profile between the upper and lower X-point is turned into a straight line in order to allow for a placement of the bucking cylinder and the central solenoid. The elliptic and straight inner leg segment of the TF coil are defined by

$$\left(\frac{r-R}{a_1}\right)^2+\left(\frac{z}{b}\right)^2=1 \quad \text{for} \quad R_1<r\le R$$
$$r=R_1 \quad \text{otherwise} \tag{17}$$

where a_1 and b are the horizontal and vertical semi-axis of the inner ellipse, respectively, R is the plasma major radius, and R_1 is the inboard radius that corresponds to the outer contour of the TF coil. Similarly, the outer leg is described by

$$\left(\frac{r-R}{a_2}\right)^2+\left(\frac{z}{b}\right)^2=1 \quad \text{for} \quad r>R \tag{18}$$

where a_2 is the horizontal semi-axis of the outer ellipse. The semi-axes of the inner and outer leg are obtained by fitting the TF coil shape to the ARIES-AT coil and depend on the plasma major radius R, inboard and outboard radii of the outer contour of the TF coil (R_1 and R_2) and the height of the X-point z_{xp} as

$$a_1=\frac{R-R_1}{\sqrt{1-\left(z_{xp}/b\right)^2}}$$
$$a_2=R_2-R \tag{19}$$
$$b=0.5H_{VV}+\delta_v$$

where H_{VV} is the height of the vacuum vessel and $\delta_v=1\,m$ is the clearance between the vacuum vessel and the TF coil at the vertical axis. The inboard radius of the outer contour (R_1) is determined by the inboard radial build of the power core elements until the bucking cylinder. The outboard radius of the outer contour (R_2) is

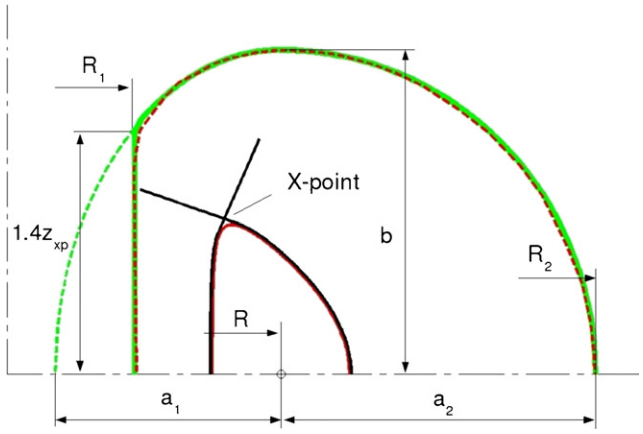

Fig. 3. Shape of the TF coil modeled by the ARIES systems code (full green contour) compared to the reference shape (red dashed) used in the ARIES-AT reactor. (For interpretation of the references to color in this figure legend, the reader is referred to the web version of the article.)

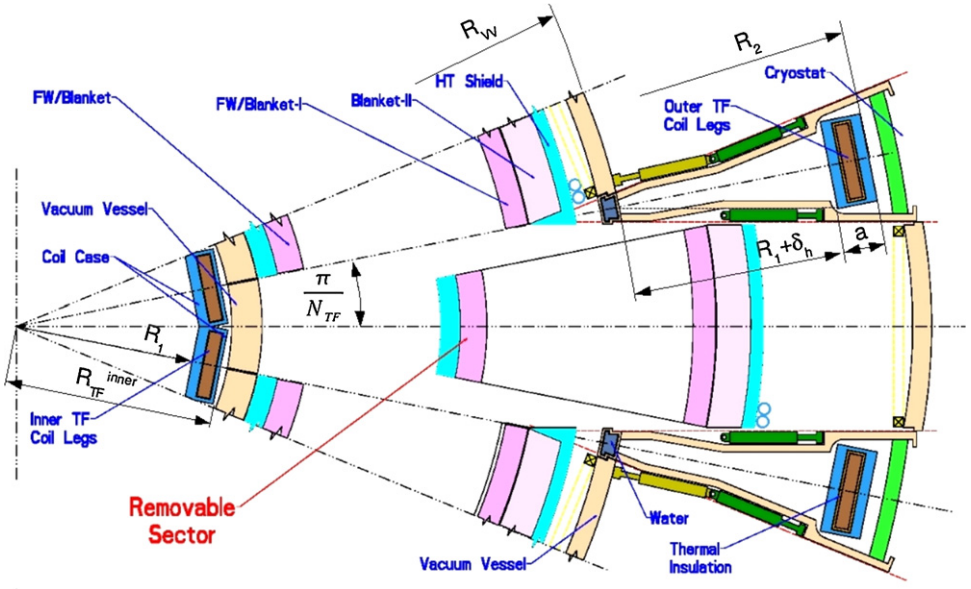

Fig. 4. Plan view of the removable power core sector of the ARIES-AT as it is being withdrawn for maintenance.

estimated based on the requirement that the clearance between the TF coils on the outboard side allows for removal of the power core segments for maintenance purpose, as shown in Fig. 4:

$$R_2 = R_{VV} + R_1 + \delta_h + a \tag{20}$$

where R_{VV} is the outmost radius of the vacuum vessel at $z = 0$, a is the thickness of the TF coil, $\delta_h \simeq 10\,\mathrm{cm}/\sin(\pi/N_{TF})$ is the radial distance needed to provide a $\simeq 10$ cm clearance for the maintenance port, and N_{TF} is the number of TF coils.

For a given superconductor, the cross-sectional areas of the cable components are estimated based on the specified toroidal magnetic field at plasma major radius and the nominal electric current of $I_{TF} = 40\,kA$. The cable is composed from arrays of strands, which are embedded into a coil casing made of a structural material such as SS316 or Japanese austenitic steel with low carbon and boron (JK2LB). The superconductor is typically accompanied by a stabilizer (Cu), coolant, insulator and a thin protective sheath (usually made of Inconel).The procedure for estimating the cross sectional areas of conductive components is based on the current density at the location of the maximum magnetic field. Fig. 5 shows this dependence for several superconductors of interest in the advanced tokamak studies. The maximum magnetic field is determined at the inboard radius of the inner contour of the TF coil R_{TF}^{inner}, shown in Fig. 4

$$B_T^{\max} = \frac{B_T R}{R_{TF}^{inner}} \tag{21}$$

The procedure for calculating the cross sections of the coil components is described in the following text for two example superconducting material models of the TF magnet.

4.2.1.1. High temperature superconductor (YBCO). Components, material properties and costs of the high temperature superconductor are given in Table 8. Given the value of $B_T^{\max}$, the current density in the superconductor is obtained by interpolation from the experimental curve that corresponds to YBCO, shown in Fig. 5:

$$J_{SC} = f_{YBCO}(B_T^{\max}) \tag{22}$$

The current density in the stabilizer (Cu) is

$$J_{Cu} = \frac{J_{SC}}{2} \tag{23}$$

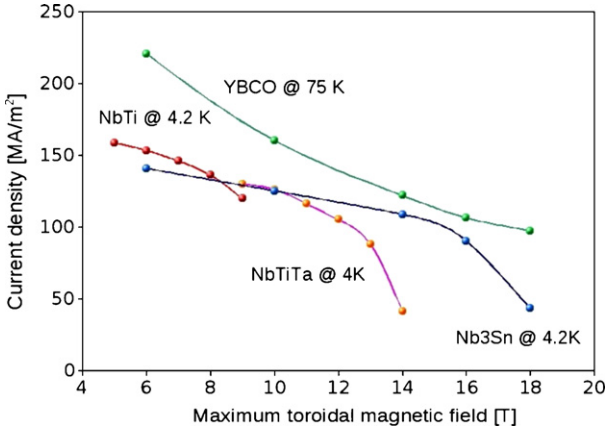

Fig. 5. Current density versus maximum magnetic field for different superconductors commonly used for tokamak magnets.

The cross sectional areas of the conductive components are

$$\begin{aligned} A_{SC} &= \frac{I_{TF}}{J_{SC}} \\ A_{Cu} &= \frac{I_{TF}}{J_{Cu}} \\ A_{cond} &= A_{SC} + A_{Cu} \end{aligned} \tag{24}$$

The area of the single cable in the winding pack is estimated by taking into account the area fractions that correspond to the liquid nitrogen coolant (φ_{He}), insulator (φ_{ins}) and sheath (φ_{sheath}):

$$A_{cable} = \frac{A_{cond}}{1 - \varphi_{He} - \varphi_{sheath} - \varphi_{ins}} \tag{25}$$

The area fraction of the sheath follows from the requirement that the hoop stress does not exceed the allowed limit for Inconel at cryogenic temperatures ($\sigma_{hoop}^{\max} = 1600\,\mathrm{MPa}$):

$$\varphi_{sheath} = 1 - \left(1 - \frac{(B_T^{\max})^2}{2\mu_0\sigma_{sheath}}\right)^2 \tag{26}$$

where $\mu_0 = 4\pi \times 10^{-7}$ is the magnetic permeability and $\sigma_{sheath} = 0.5\sigma_{hoop}^{\max}$. The cross sectional areas of the coolant, insulator and sheath can now be retrieved by multiplying the cable area by their respective fractions. The total area of the winding pack is $A_{wp} = N_{wp} \cdot A_{cable}$, where N_{wp} is the number of turns per winding pack in a single TF coil calculated by the formula

$$N_{wp} = \frac{B_T^2 \pi R}{N_{TF} I_{TF} \mu_0} \tag{27}$$

Having obtained the cross sectional areas of all of the components of the winding pack, the next step is to estimate the amount of structural material needed to support the TF coil. This is a non-trivial task given the complexity of the 3D magnetic loads imposed by the electric current in the TF coil and the surrounding TF and PF magnets. A structural analysis integrated into the algorithm would be beyond the current scope of the systems code. For that reason, an approximation for the TF coil thickness was adopted by scaling a formula based on bending stress in elastic beams to the reference thickness obtained by a highly accurate finite element analysis of the ARIES-AT coil, Ref. [13]. The total thickness of the TF coil obtained by this approach is

$$a = 0.208 \cdot \sqrt{\frac{3}{16\sigma_b\mu_0}} \cdot \frac{B_T R}{R_2 - R_1} \cdot \sqrt{(R_2^2 - R_1^2)\left(1 + \ln\left(\frac{R_2}{R_1}\right)\right) + R_1 R_2 \left(2 - \ln^2\left(\frac{R_2}{R_1}\right)\right)} \tag{28}$$

where σ_b is the maximum allowed bending stress in the structural material, listed in Table 8.

The total cross sectional area needed for estimating the volume fractions of the components of the TF coil is

$$A_{TF} = a\frac{2\pi R_1}{N_{TF}} \tag{29}$$

Assuming that the coil cross section is uniform along the perimeter, the volume fractions of all the components can now be estimated as

$$f_i = \frac{A_i N_{wp}}{A_{TF}} \tag{30}$$

where i denotes the component including SS316, YBCO, Cu, Inconel, insulating polymer and liquid nitrogen.

Table 8
Components, material properties and costs of the high temperature (T) and low temperature magnet.

Material	Name	Density [kg/m^3]	Unit cost [$/kg]	Cost base year	Max. allowed stress [MPa]	Type of magnet
Stainless steel 316	SS316	7860	68.657	1992	900	high T
Japanese Austenitic Steel	JK2LB	8000	30.0	2004	400	low T
Superconductor	YBCO	6200	92.7	1992		high T
Superconductor	NB3SN	7500	500.0	2007		low T
Stabilizer	Cu	7300	65.4	1992		high or low T
Structure	Inconel	8400	50.912	1992	1600	high or low T
Structure	JK2LB	8400	50.912	1992	1600	low T
Insulator	Polyimide	1920	16.516	1992		high or low T

4.2.1.2. Low temperature superconductor (Nb_3Sn). The relevant material properties for the low temperature superconductor coil components are shown in Table 8. The nitrogen coolant is replaced with helium for these magnets. The procedure for obtaining the cross sections of the components is similar to the example described above, except for the following details. For a given value of $B_T^{\max}$, the current density in the superconductor is obtained from an empirical dependence

$$J_{SC} = \left[-0.0908\left(B_T^{\max}\right)^2 + 1.0224B_T^{\max} + 12.32\right] \times 10^8 [A/m^2] \tag{31}$$

The current density in the stabilizer is optimized in order to expedite the dissipation of heat generated during accidental quenching of the superconductor,

$$J_{Cu} = \sqrt{\frac{2J_{2\tau}}{\tau}} \tag{32}$$

where $J_{2\tau} = 5 \times 10^{16} \mathrm{A^2 s/m^4}$ is a term proportional to the heat dissipation and $\tau = 2s$ is the dissipation time. The remainder of the procedure for obtaining the volume fracture of the TF coil component is identical to the one used for the high temperature superconductor.

4.2.1.3. Costing of the TF coil. The total cost of the TF coil is calculated by summing up the costs of all of its components,

$$c_{TF\,coil} = V_{TF\,coil} \cdot \sum_{i=1}^{n} c_i \xi_{inf}(Y_i, Y_{current})\, \rho_i f_i \tag{33}$$

In this expression, the cost of an individual component i is the product of the cost per unit mass c_i, density ρ_i, volume fraction f_i, and the total volume of the TF coil $V_{TF\,coil}$. The inflation is taken into account by the conversion factor $\xi_{inf}(Y_i, Y_{current})$, where Y_i is the cost base year and $Y_{current}$ is the current year. As an alternative to the Eq. (33), the ARIES systems code allows for an option of estimating the cost of the cable based on the bulk cost per unit cable length, which is 260 $/m in case of Nb_3Sn. In this case, the total cost of the TF magnet is estimated by adding the cost of the cable to the cost of the structure, stabilizer, and insulator. This is a conservative approach, used in order to achieve a more realistic near-term estimate.

4.2.2. Poloidal field magnet algorithm

The poloidal field (PF) magnet consists of 36 coils; 8 of these are placed along the inner radius of the bucking cylinder and comprise the central solenoid, as shown in Fig. 6, while the remaining coils are evenly distributed along the outer surfaces of the toroidal field caps. In the actual design, the number of PF coils may be reduced with fewer larger coils. The location of the outermost coil is limited by the vertical distance of the maintenance port opening. The thickness of a PF coil in the poloidal cross section is determined by the current required in the coils, maximum current density in the superconductor and structural requirements.

The present algorithm consists of the following steps:

1. Estimate the coil currents at the zero flux state. In the present approximation they are assumed to be known and taken as an input, based on ARIES-I and ARIES-AT PF coil solutions.
2. Scale the coil currents from their values at the zero flux state to the values at the given plasma edge safety factor q_{95} and the plasma current I_P.
3. Determine the cross sectional areas of different components by the procedure outlined in Section 4.2.1. for the low temperature superconductor Nb_3Sn. The maximum current in the PF coil is calculated by taking into account the flux swing required to ramp up the plasma current from zero to the value required for the given operating point.
4. Estimate the amount of the structural material needed (SS316 in the current algorithm) based on the hoop stress limit.
5. Place the coils uniformly on the outer surface of the bucking cylinder and the toroidal caps.
6. Integrate the cost across the volume of the each individual coil, by using the Eq. (33).

4.3. Blankets

Two example blanket concepts are incorporated in this initial version of the new ARIES system code: an advanced LiPb/SiC blanket, which was developed as part of the ARIES-AT study [10]; and a dual coolant lithium lead (DCLL) blanket more recently employed in the ARIES-CS study [32]. The algorithms for both blanket concepts are described in this paper for completeness. However, the

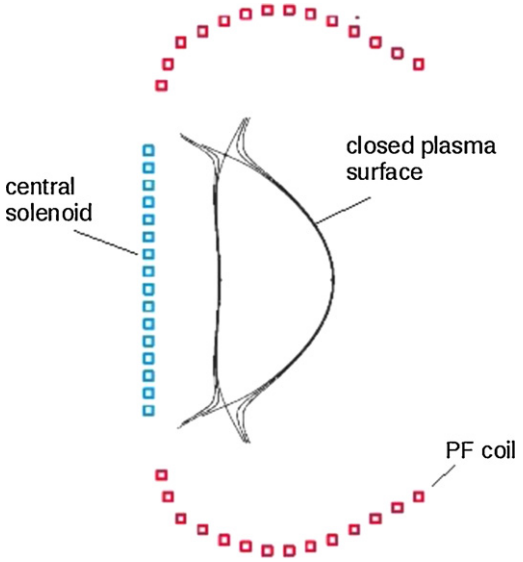

Fig. 6. Poloidal field coils.

Table 9
Summary of Brayton power cycle parameters assumed for the systems code analysis.

Brayton cycle parameter	Value
Number of compression stages	3
Number of expansion stages	1
HX temperature difference between hot and cold legs	30 °C
Compressor efficiency	0.89
Turbine efficiency	0.93
Recuperator effectiveness	0.95
Total compression ratio	< 3.5
Cycle lowest He temperature	35 °C
Fractional cycle He pressure drop	0.045
Cycle He pressure	15 MPA

example results shown in the paper focus on the ARIES-AT Pb–17Li + SiC_f/SiC blanket.

4.3.1. Self-cooled Pb–17Li + SiC_f/SiC blanket

The blanket utilizes Pb–17Li as a breeder and coolant and a low-activation SiC_f/SiC composite as a structural material [10]. The blanket is coupled to a Brayton cycle (with He as a working fluid and described in Section 5.2) through a heat exchanger (Table 9). The Pb–17Li operating temperature is optimized to exit at 1100 °C in order to provide high power cycle efficiency while maintaining the SiC_f/SiC temperature under 1000 °C.

4.3.2. DCLL blanket

The dual coolant concept utilizes He to cool the ferritic steel structure, including the first wall. The Pb–17Li channels are lined with a SiC flow channel insert (FCI) that allows high temperature (~700 °C) Pb–17Li in the channel. In this power plant configuration, the divertor is also cooled by He.

5. Power flow

The power flow schematic of the current steady state tokamak chamber model is depicted in Fig. 7. The fusion power is generated in the plasma in the form of neutrons and alpha particles, where neutrons escape the plasma and enter the surrounding structures and coolants. The alpha particles are trapped inside the plasma and heat the plasma. These two sources of heat are transmitted to the power conversion system via several mechanisms. The power from neutrons is directly absorbed by the first wall, blanket, divertor and HT shield. The neutron and gamma energies are deposited into the structure and liquid Pb–17Li, which serves as a coolant (heat transfer media) and a tritium breeder. As a result, the source neutron energy increases by 10–20% depending on the blanket concept, yielding a neutron energy multiplication of 1.1-1.2. A portion of the power from the alpha particles is radiated from the plasma to the first wall and divertor while the remainder is conducted to the divertor via charged particles.

In the power flow algorithm, the core elements are separated into two functional groups, as shown in Fig. 7. The neutron power deposition split is described below.

1. *First wall, blankets and high-temperature (HT) shields* receive the fractions of the neutron (and plasma core radiation power) that are roughly proportional to the coverage area of the first wall. The total power absorbed by this group is split between the inboard (40%) and the outboard section (60%) based on the ratio between the corresponding plasma-facing areas. Within each of these sections, the first wall and blanket receive 90% of the neutron power while the HT shield receives 10%. Details about the alpha power deposition and split are described in Section 5.1.
2. *Divertor system* absorbs the remainder of the fusion power. A fraction of 90% of the neutron power is assumed to be deposited in the divertor plates and 10% in the divertor shield. The above assumptions for the fusion power distribution among the power core groups are compatible with the ARIES-AT design [10].

The thermal power collected within the power core coolant is transferred to the power cycle via a heat exchanger, as described in Section 5.2.

The electric power output from the conversion system described above (gross electric power) is reduced by the amount needed to operate the blanket and divertor coolant pumps (mainly for He), current drives and various auxiliary plant functions, such as maintaining the cryogenic temperatures of the magnets, etc. The remaining net electric power is the output to the electric grid.

5.1. Plasma power flow

The component of the fusion power stored in the alpha particles (P_α) is estimated in the physics module of the ARIES systems code. Based on this quantity, the neutron and fusion power are obtained as

$$P_{neutron} = P^{DT}_{neutron} + P^{DD}_{neutron}$$
$$P_{fusion} = P_{neutron} + P_\alpha \quad (34)$$

where $P_{neutron}$ is the neutron power with components $P^{DT}_{neutron}$ and $P^{DD}_{neutron}$ originating from the deuterium-tritium and deuterium-deuterium reactions, respectively, and P_{fusion} is the fusion power. In order to maintain the plasma at a steady state, an auxiliary power P_{aux} must be supplied to the plasma, partially as a current drive power (P_{CD}, Eq. (8)) and partially to support additional heating of the plasma ($P_{plasma\,heating}$). The power stored in the alpha particles and the auxiliary power comprise the plasma power:

$$P_{plasma} = P_\alpha + P_{aux} \quad (35)$$

The plasma power is transferred out of the closed plasma surface by plasma particles and radiation to the first wall ($P_{rad\,chamb}$) which can include direct alpha particle losses to the first wall,

$$P_{plasma} = P_{particle} + P_{\alpha\,loss} + P_{rad\,chamb} \quad (36)$$

where $P_{particle}$ is the power of the plasma particles that leave the plasma and $P_{\alpha\,loss}$ is the portion of the total power stored in alpha particles that is lost (in the advanced tokamak designs considered in this study, it is assumed that no such loss occurs). After leaving the plasma, the plasma particles transfer a portion of their power to divertor via conduction ($P_{cond\,div}$) and the rest is radiated to the divertor walls ($P_{rad\,edge}$):

$$P_{particle} = P_{cond\,div} + P_{rad\,edge} \quad (37)$$

The latter term is estimated as

$$P_{rad\,edge} = f_{div\,rad} \cdot P_{particle} \quad (38)$$

where $f_{div\,rad}$ is a coefficient that determines the fraction of power radiated in the divertor, specified in Table 4. The present assumption is that 90% of the $P_{rad\,edge}$ arrives at the divertor while 10% is absorbed by the first wall. The total radiated power from the plasma core is estimated in the physics module of the ARIES systems code as

$$P_{rad\,chamb} = P_{brem} + P_{cycl} + P_{line} \quad (39)$$

where P_{brem} is the Bremsstrahlung radiation loss, provided in the Eq. (5), P_{cycl} is the cyclotron radiation loss and P_{line} is the line radiation loss, provided in the Eq. (6). The fraction of the radiated power from the chamber that arrives at the divertor plates is proportional to a geometry factor defined as $f_{geo\,div} = A_{div}/(A_{FW} + A_{div})$, where A_{div} is the total area of the divertor plates and A_{FW} is the total area

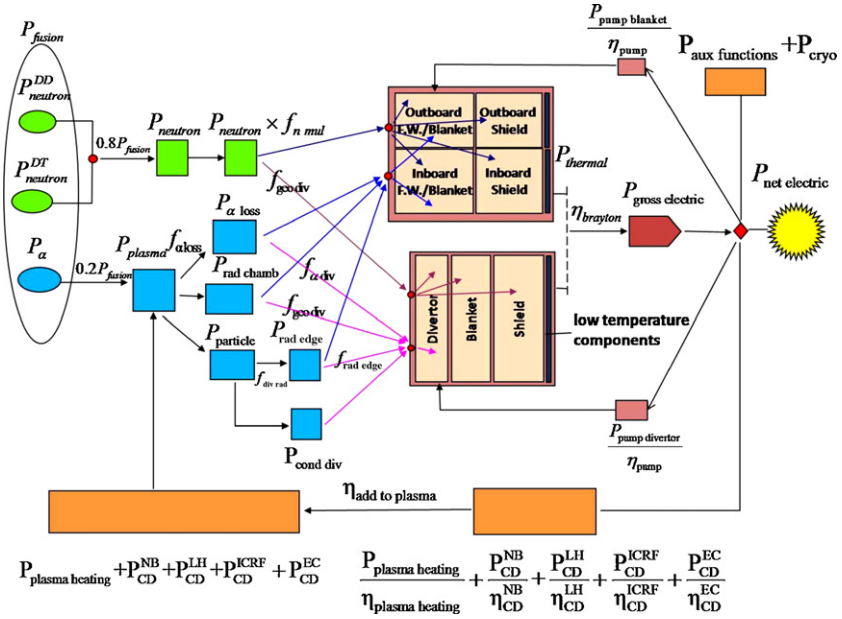

Fig. 7. Power flow in a steady state tokamak.

of the first wall. The majority of the $P_{rad\,chamb}$ quantity is absorbed by the first wall, as shown in Fig. 7.

5.2. Power cycle

Different power cycles are available for electrical production, including the Rankine steam cycle and the Brayton cycle. The latter is particularly attractive for high temperature cases since it provides the possibility of higher efficiency. The Brayton cycle is chosen for the present power plant model since the power core designs under consideration operate with high coolant temperatures (up to ~1000–1100 °C for the ARIES-AT case and ~700–800 °C for the ARIES-CS DCLL case). The Brayton cycle considered for inclusion in the system code includes 3 compression stages and a single expansion stage, as illustrated in Fig. 8.

For both the ARIES-AT and the DCLL blanket cases, parametric thermal-hydraulic analyses were performed to assess their performances when coupled with this Brayton cycle through a heat exchanger. Details of these can be found in Refs. [10] and [32], respectively.

Here, key aspects of the analysis are summarized and the results used as input in the system code are listed.

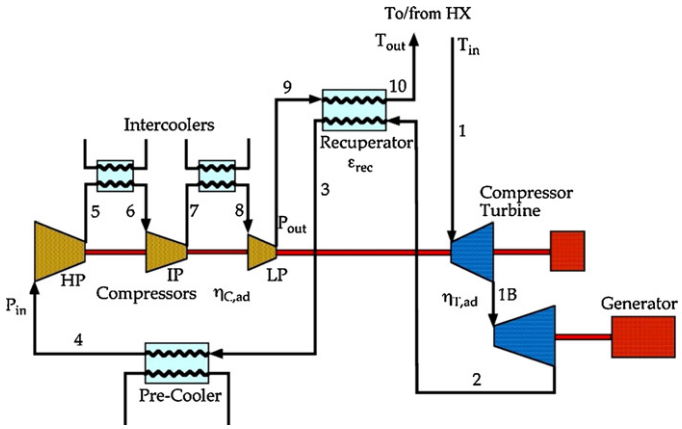

Fig. 8. Brayton cycle considered in this analysis.

5.2.1. ARIES-AT blanket coupled to Brayton cycle

The analysis was done by adjusting the thermal–hydraulic parameters to optimize the thermal efficiency for different heat load cases (neutron wall load and surface heat flux) based on given material constraints. The fusion power was kept constant and the machine size was varied to adjust the neutron wall load. The following parameters and constraints were assumed for the analysis [10]:

- Fusion power = 1.74 GW
- Maximum/Average neutron wall load peaking factor=1.5 [19]
- Maximum/Average plasma heat flux to first wall peaking factor=1.25
- Maximum allowable combined stress in SiC_f/SiC = 190 MPa
- Maximum allowable SiC_f/SiC temperature = 1000 °C
- Maximum allowable CVD SiC temperature=1000 °C

The results for the cycle gross efficiency and blanket pumping power are summarized in Figs. 9 and 10 as a function of maximum neutron wall load and maximum surface heat flux. The highest values shown for these are close to the design limits and system

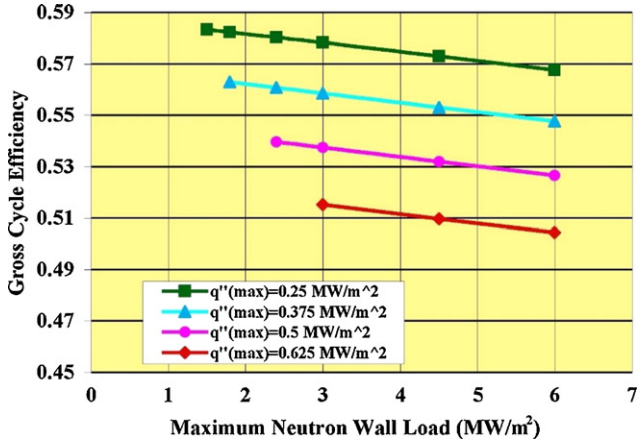

Fig. 9. Gross cycle efficiency as a function of maximum neutron wall load and maximum plasma heat flux for ARIES-AT like blanket coupled to a Brayton cycle.

code cases should fall within these limiting values (~6/4 MW/m^2 as maximum/average neutron wall load and ~0.625/0.5 MW/m^2 as maximum/average plasma heat flux to the first wall). In the ARIES-AT power plant conceptual design, both the blanket and divertor are made of SiC$_f$/SiC and cooled with Pb–17Li. The presence of low-conductivity SiC helps minimize MHD effect and the resulting pressure drop and pumping power are quite small.

5.2.2. DCLL blanket coupled to Brayton cycle

A similar thermal-hydraulic analysis was done for the DCLL blanket of ARIES-CS [32]. In these calculations, the friction power from the He flow in the blanket and divertor (~90% of the pumping power) was added to the fusion thermal power. The thermal-hydraulic parameters of the power core were then optimized to maximize the net cycle efficiency (based on the gross electrical power minus the pumping power) for the following set of parameters and material constraints [32]:

- Fusion power = 2.37 GW
- Maximum/Average neutron wall load peaking factor for tokamaks = 1.5 [30]
- Maximum/Average plasma heat flux peaking factor = 1.25
- Overall thermal conductance SiC insert region = 200 W/(m^{2}K)
- Maximum allowable temperature for reduced activation ferritic steel (RAFS) = 550 °C
- Maximum allowable temperature for oxide-dispersion strengthened ferritic steel (ODS – FS) = 700 °C
- Maximum allowable Pb–17Li/RAFS interface temperature (compatibility limit) = 500 °C

The fusion power was kept constant and the machine size was varied to adjust the neutron wall load and surface heat flux. The results for the cycle gross efficiency and blanket pumping power are shown in Figs. 11 and 12. Again, the highest values shown for these are an indication of the design limits and system code cases should fall within these limiting values (~5/3.3 MW/m^2 as maximum/average wall load and ~1/0.8 MW/m^2 as maximum/average plasma heat fluxes).

In the DCLL case, He is used to cool the blanket structure and the divertor and the resulting pumping power is substantial. This is illustrated in Fig. 12 for the blanket. In addition, the divertor pumping power is included in the system code normalized to the divertor coverage (= (0.3416 × Area$_{\text{divertor}}$ [m^2]) MW). The change in slope observed for both the gross efficiency and the blanket pumping power (shown in Figs. 11 and 12) as the maximum neutron wall load is reduced can be explained by a shift in the governing constraints. For a given maximum surface heat flux, the RAFS maximum allowable temperature at the FW (<480 °C) tends to govern the results at high wall loads and as the wall load is reduced at some point the maximum Pb–17Li/SiC interface temperature in the back of the blanket (<500 °C) becomes the governing factor.

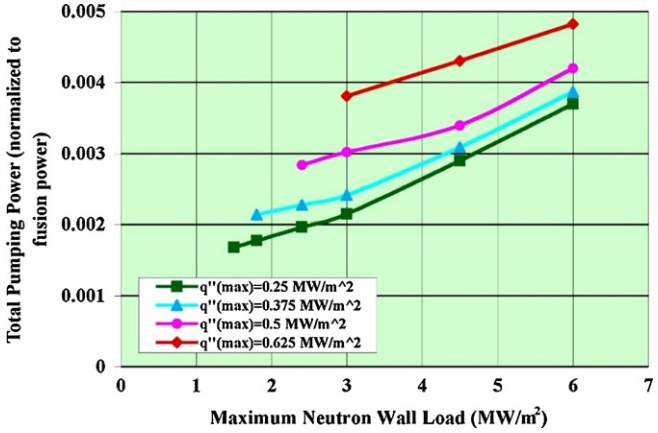

Fig. 10. Total normalized pumping power (blanket + divertor) as a function of maximum neutron wall load and maximum plasma heat flux for ARIES-AT Pb–17Li blanket coupled to a Brayton cycle.

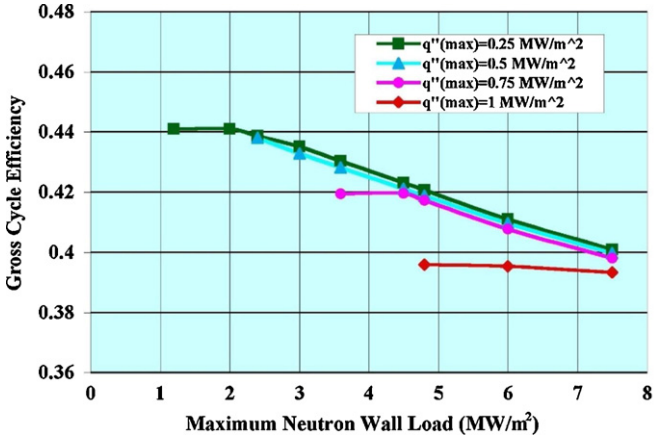

Fig. 11. Gross cycle efficiency as a function of maximum neutron wall load and maximum plasma heat flux for a DCLL blanket coupled to a Brayton cycle.

6. Engineering filters

In order to keep the tokamak power plant model within desired operational and safety limits, the engineering module of the ARIES systems algorithm filters out all the design points that do not meet the following criteria:

- Toroidal magnetic fields in the TF and PF coils, respectively, are limited by material and plasma confinement requirements as shown in Eq. (40):

$$6.0\,T < B_T^{TF\,coil} < 18.0\,T$$
$$B_T^{PF\,coil} < 18.0\,T \quad (40)$$

- Heat flux to divertor is limited by the material properties of divertor plates and coolant combination, see Eq. (41):

$$q_{div}^{inboard} < Q_{div\,lim}$$
$$q_{div}^{outboard} < Q_{div\,lim} \quad (41)$$

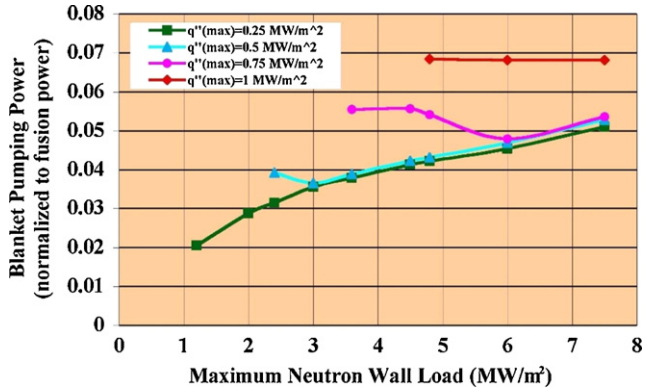

Fig. 12. Normalized blanket pumping power as a function of maximum neutron wall load and maximum plasma heat flux for a DCLL blanket coupled to a Brayton cycle.

where $q_{div}^{inboard}$ is the peak heat flux that reaches the divertor plates that are located on the inboard side of the X-point; $q_{div}^{outboard}$ is the peak heat flux received by the outboard divertor plates; $Q_{div\,lim}$ is the limiting value of the heat flux from both conduction and radiation, which is currently assumed to be about 5–8 MW/m^2 for the ARIES-AT LiPb cooled, W-faced SiC structure divertor case [10] and about 10–12 MW/m^2 for the He-cooled W alloy divertor case, similar to that of ARIES-CS [32]. The estimate of the peak heat flux reaching the divertor plate is based on the power scrape off width [33], the divertor geometry and the assumed radiated power fraction in the divertor.

- Neutron wall load ($q_{NWL}^{\max}$) and maximum surface heat flux on the first wall (q''^{max}) are limited by the constraints discussed in Section 5.2, which for the ARIES-AT Pb − 17Li + SiC$_f$/SiC blanket case are:

$$\begin{aligned} q_{NWL}^{\max} &< 6.0\,\mathrm{MW/m^2} \\ q''^{max} &< 0.63\,\mathrm{MW/m^2} \end{aligned} \tag{42}$$

For the DCLL blanket, the upper limits for $q_{NWL}^{\max}$ and q''^{max} are 10.0 MW/m^2 and 1.0 MW/m^2, respectively.

- Net electric power can depart by no more than 5 MW from the reference value of 1000 MW:

$$995\,MW \le P_E \le 1005\,\mathrm{MW} \tag{43}$$

7. Costing

In the ARIES systems code, the costing algorithm consists of the following steps:

1. Calculate the mass-dependent costs of the power core elements. These costs are obtained by summing the products of the unit costs adjusted for inflation, volumes, fractional densities, and densities of different material components [$/kg] for the volume of each component, as for example given by Eq. (33) for the coils.
2. Estimate the direct costs for the other power plant systems, subsystems and components by using the algorithms given in Section 7.1.
3. Sum up the direct costs and calculate the indirect costs of the power plant by using the algorithms given in Section 7.2.
4. Estimate the cost of electricity, as given in Section 7.3.

The top level accounts of the high-level costing structure currently used in the ARIES systems code are listed in Table 10 along with their corresponding LSA factors as recommended by Delene [16] and Bathke [18]. Here, the direct costs are estimated in the accounts 20–27, their sum is the output of the account 90, while the indirect costs are represented by the accounts 91–98. The total capital cost is evaluated by summing up the direct and indirect costs and provided in the account 99. The level of safety assurance (LSA) as developed by Holdren et al. [35,36] has an impact on both direct and indirect costs by the savings derived from substitution of conventional for nuclear safety-grade components and by elimination of some of the active safety systems, depending on the level of inherent safety demonstrable by the tokamak power plant. These savings are accounted for by applying the cost credit factors, shown in Table 10, to the outputs of the costing accounts. Details of calculating direct costs, indirect costs and cost of electricity will be provided in the following subsections.

7.1. Direct costs

The algorithms for calculating direct costs incorporate the previously obtained mass-dependent costs of many of the power core elements. The remaining elements depend on other relevant quantities, such as power or surface area. In general, such costs are estimated by evaluating the expression of the form $c_i \cdot (X_i)^{e_i}$, where c_i is the unit cost for the costing account i (given in $/kg, $/W, $/m^2, etc.), X_i is the quantity the cost is proportional to and e_i is the cost-scaling exponent that accounts for the costs of nuclear safety grade components, typically used in advanced fission reactors and modified for fusion applications [37]. In the costing algorithms, both the unit cost and the corresponding quantity may be adjusted for manufacturing expenses, assuming an advanced technology of the future and extrapolating to a high performance creadible power plant.

The algorithms for estimating the direct costs are taken from the original systems code and summarized in Tables 11–13 that reflect the ARIES-AT economics [38]. The costing accounts have an expandable multi-level structure. The lowest level accounts return the costs calculated by summing up the previously obtained mass-dependent costs, such as the account 22.1.1 in the Table 12, or from other appropriate expressions, such as the account 22.2.1. In the former example, the input variables for the account 22.1.1 are the costs of the first wall and blankets that are estimated by the power core algorithm of the systems code. In the latter example, the input variable is the thermal power, which originates from the power flow circuit algorithm. The impact of the LSA on the output of the costing account i takes place via multiplication by the cost credit factor $\xi_i(LSA)$. All of the accounts of the same level are summed up to produce the cumulative output for a higher level account as shown in Table 12, for the accounts 22.0, 22.1, 22.2 and 22.5. The only exception from this rule is when all of the sub-accounts are temporarily set to zero, such as those listed in Tables 11 and 13. In such cases, the top level account is treated as the lowest level account and returns the cost based on an appropriate expression. The sub-accounts with null outputs, shown here for completeness, are currently being developed as an effort to achieve a more accurate partition of costs and will have non-trivial outputs in the future.

7.2. Indirect costs

The indirect costs are represented by the costing accounts 90-99, as shown in Table 10. The account 90 provides the total direct cost (TDC) by summing up the top level accounts 20–27:

$$c_{90} = \sum_{i=20}^{27} c_{i.0} \tag{44}$$

The accounts 91. "Construction services and equipment", 92. "Home office engineering and services" and 93. "Field office engineering and services"are all proportional to the total direct cost and depend on the level of safety assurance as

$$c_j = c_{90} \cdot \xi_j(LSA) \tag{45}$$

where j is either 91, 92 or 93 and $\xi_j(LSA)$ is the cost credit factor that corresponds to the account j, shown in Table 10. The sum of the total direct cost and the indirect costs provided by the accounts 91–93 is the owner's cost:

$$c_{94} = (c_{90} + c_{91} + c_{92} + c_{93})\,\xi_{94}(LSA) \tag{46}$$

The process contingency (account 95) and project contingency (account 96) are estimated by the formula

$$c_j = (c_{90} + c_{91} + c_{92} + c_{93} + c_{94}) \cdot \xi_j(LSA) \tag{47}$$

Table 10
Overview of the costing accounts used in the ARIES systems code and corresponding cost credit factors for different levels of safety assurance [34].

Number	Costing account	Level of safety assurance			
		1	2	3	4
Direct costs					
20.	Land and land rights	1.00	1.00	1.00	1.00
21.	Structures and site facilities				
	Reactor building and hot cell buildings	0.60	0.90	0.96	1.00
	Turbine - generator building	1.00	1.00	1.00	1.00
	Other structures and improvements	0.60	0.67	0.67	1.0
22.	Reactor plant equipment				
	Fusion energy capture and conversion	0.90	0.95	1.00	1.00
	Plasma confinement (TF, PF, CF)	0.90	0.95	1.00	1.00
	Heat transfer and transport				
	- with intermediate heat exchanger (IHX) or He with double walled steam generator	0.60	1.00	1.00	1.00
	- with other options	0.90	1.00	1.00	1.00
	All other reactor plant equipment	0.85	0.94	0.94	1.00
23.	Turbine plant equipment	1.00	1.00	1.00	1.00
24.	Electric plant equipment	0.75	0.84	0.84	1.00
25.	Miscellaneous plant equipment	0.85	0.90	0.93	1.00
26.	Heat rejection system	1.00	1.00	1.00	1.00
27.	Special materials	1.00	1.00	1.00	1.00
Indirect costs					
90.	Total direct cost (not including contingency)	1.000	1.000	1.000	1.000
91.	Construction services and equipment	0.113	0.120	0.128	0.151
92.	Home office engineering and services	0.052	0.052	0.052	0.052
93.	Field office engineering and services	0.052	0.060	0.064	0.087
94.	Owner's cost	0.150	0.150	0.150	0.150
95.	Process contingency	0.000	0.000	0.000	0.000
96.	Project contingency	0.150	0.173	0.184	0.195
97.	Interest during construction (IDC)	1.000	1.000	1.000	1.000
98.	Escalation during construction (EDC)	1.000	1.000	1.000	1.000
99.	Total capital cost (TCC)	1.000	1.000	1.000	1.000
Operations and maintenance cost (O&M)		0.700	0.850	0.925	1.000
Decontamination and decommissioning allowance (D&D), mill/kWeh, constant $.		0.250	0.500	0.750	1.000

where j is either 95 or 96. For a mature, high performance creadible power plant, the process contingency is omitted from consideration (i.e. $\xi_{95}(LSA) = 0$). The interest during construction is calculated in the account 97 as

$$c_{97} = f_{IDC} \cdot c_{90} \tag{48}$$

where $f_{IDC} = 0.2821$ is the nominal factor for interest during construction [40,41], estimated assuming the average cost of money of 6.05% (without inflation) or 11.35% (with inflation). The construction time period is nominally considered to be 6 years with a skewed S-shaped expenditure curve. The escalation during construction (account 98) is currently neglected in the constant cost of money calculation but will be included in the nominal cost of money calculation to be utilized at a future date. The total capital cost is a sum of all the direct and indirect costs:

$$c_{99} = \sum_{i=90}^{98} c_i \tag{49}$$

Table 11
Accounts 20 and 21.

Number	Account title	Cost [M$ 1992] Ref. ARIES-AT
20.0	Land and land rights [a]	$c_{20.0} = \sum_{i=1}^{2} c_{20.i} \cdot \xi_{20.0}(LSA)$
20.1	Land and privilege acquisition	$c_{20.1} = 10.0$ (TBD)
20.2	Relocation of buildings, utilities, highways, etc.	$c_{20.2} = 0.589$ (TBD)
21.0	Structures and site facilities	$c_{21.0} = \sum_{i=1}^{9} c_{21.i}$
21.1	Site improvements and facilities	$c_{21.1} = 18.707 \cdot \xi_{21.1}(LSA)$
21.2	Reactor building [b]	$c_{21.2} = 78.09 \cdot \left(\frac{V_{rb}}{80{,}000}\right)^{0.62} \cdot \xi_{21.2}(LSA)$
21.3	Turbine building [c]	$c_{21.3} = (30.63 \cdot \left(\frac{P_{ET}}{1200}\right)^{0.75} + 6.11) \cdot \xi_{21.3}(LSA)$
21.4	Cooling structures [c]	$c_{21.4} = 12.47 \cdot \left(\frac{P_{ET}}{1000}\right)^{0.3} \cdot \xi_{21.4}(LSA)$
21.5	Power supply and energy storage building	$c_{21.5} = 16.0 \cdot \xi_{21.5}(LSA)$
21.6	Miscellaneous buildings	$c_{21.6} = 133.63 \cdot \xi_{21.6}(LSA)$
21.7	Ventilation stack	$c_{21.7} = 3.16 \cdot \xi_{21.7}(LSA)$
21.8	Spare parts allowance	$c_{21.8} = 8.285 \cdot \xi_{21.8}(LSA)$
21.9	Contingency allowance	$c_{21.9} = 0$ (TBD)

[a] Cost credit factors ξ_i that correspond to the given level of safety assurance (LSA) are listed in Table 10.
[b] $V_{rb} = (R_{cryo} + 9)^2 \cdot 6H_{cryo} + 1.55 \times 10^5$- reactor building volume [m^3]. R_{cryo} [m] and H_{cryo} [m] are the radius and height of the cryogenic vessel, respectively.
[c] P_{ET}- gross electric power [MW].

Table 12
Account 22.

Number	Account title	Cost [M$ 1992] Ref. ARIES-AT
22.0	Reactor plant equipment	$c_{22.0} = \sum_{i=1}^{9} c_{22.i}$
22.1	Reactor equipment	$c_{22.1} = \sum_{i=1}^{10} c_{22.1.i}$
22.1.1	First wall/blanket/reflector [a]	$c_{22.1.1} = (c_{FW} + c_{Blanket} + c_{Blanket\,II}) \cdot \xi_{22.1.1}(LSA)$
22.1.2	Shield [a]	$c_{22.1.2} = (c_{HT\,Shield} + c_{Div\,Shield}) \cdot \xi_{22.1.2}(LSA)$
22.1.3	Magnet coils [a]	$c_{22.1.3} = (c_{TF\,Magnet} + c_{PF\,Magnet} + c_{Bucking\,Cylinder} + c_{Toroidal\,Caps}) \cdot \xi_{22.1.3}(LSA)$
22.1.4	Supplemental heating systems [b]	$c_{22.1.4} = c_{CD} \cdot \xi_{22.1.4}(LSA)$
22.1.5	Primary structure and support [c]	$c_{22.1.5} = 0.2 \cdot V_{Prim\,Struct} \cdot \xi_{22.1.5}(LSA)$
22.1.6	Reactor vacuum system [a]	$c_{22.1.6} = c_{VV} \cdot \xi_{22.1.6}(LSA)$
22.1.7	Power supply	$c_{22.1.7} = 59.7012 \cdot \xi_{22.1.7}(LSA)$
22.1.8	Impurity control system [d]	$c_{22.1.8} = 0.078 \cdot A_{Div} \cdot \xi_{22.1.8}(LSA)$
22.1.9	Direct energy conversion	$c_{22.1.9} = 0$ (TBD)
22.1.10	ECRH breakdown system	$c_{22.1.10} = 2.78 \cdot \xi_{22.1.10}(LSA)$
22.2	Main heat transfer system	$c_{22.2} = \sum_{i=1}^{3} c_{22.2.i}$
22.2.1	Primary coolant [e]	$c_{22.2.1} = 265.98 \cdot \left(\frac{P_{TH}}{3{,}500}\right)^{0.55} \xi_{22.2.1}(LSA)$
22.2.2	Intermediate coolant system [e]	$c_{22.2.2} = 49.24 \cdot \left(\frac{P_{TH}}{3{,}500}\right)^{0.55} \xi_{22.2.2}(LSA)$
22.2.3	Secondary coolant system [e]	$c_{22.2.3} = 80.1 \cdot \left(\frac{P_{TH}}{3{,}500}\right)^{0.55} \xi_{22.2.3}(LSA)$
22.3	Auxiliary cooling systems [e]	$c_{22.3} = 1.18 \times 10^{-3} \cdot P_{TH} \cdot \xi_{22.3}(LSA)$
22.4	Radioactive waste treatment [e]	$c_{22.4} = 2.09 \times 10^{-3} P_{TH} \xi_{22.4}(LSA)$
22.5	Fuel handling and storage	$c_{22.5} = \sum_{i=1}^{7} c_{22.5.i}$
22.5.1	Pellet injection systems	$c_{22.5.1} = 12.96 \cdot \xi_{22.5.1}(LSA)$
22.5.2	Fuel processing systems	$c_{22.5.2} = 0$ (TBD)
22.5.3	Fuel storage	$c_{22.5.3} = 6.48 \cdot \xi_{22.5.3}(LSA)$
22.5.4	Atmospheric tritium recovery	$c_{22.5.4} = 0$ (TBD)
22.5.5	Water detritiation system	$c_{22.5.5} = 8.74 \cdot \xi_{22.5.5}(LSA)$
22.5.6	Blanket tritium recovery systems	$c_{22.5.6} = 8.74 \cdot \xi_{22.5.6}(LSA)$
22.5.7	Other	$c_{22.5.7} = 0$ (TBD)
22.6	Other reactor plant equipment [e]	$c_{22.6} = 1.90 \times 10^{-3} \cdot P_{TH} \cdot \xi_{22.6}(LSA)$
22.7	Instrumentation and control	$c_{22.7} = 40.90 \cdot \xi_{22.7}(LSA)$
22.8	Spare parts allowance	$c_{22.8} = 0$ (TBD)
22.9	Contingency allowance	$c_{22.9} = 0$ (TBD)

[a] c_{FW}, $c_{Blanket}$, $c_{Blanket\,II}$, $c_{HT\,Shield}$, $c_{Div\,Shield}$, $c_{TF\,Magnet}$, $c_{PF\,Magnet}$, $c_{Bucking\,Cylinder}$, $c_{Toroidal\,Caps}$ and c_{VV} are the costs of the first wall, blanket, blanket II, HT shield, divertor shield, TF magnet, PF magnet, bucking cylinder, toroidal caps, and vacuum vessel, respectively [M$ 1992].
[b] c_{CD} is the cost of the current drive system [M$ 1992].
[c] $V_{Prim\,Struct}$ is the volume of the primary structure [m^3].
[d] A_{Div} is the total area of divertor plates [m^2].
[e] P_{TH} is the thermal power [MW].

7.3. Cost of electricity

Cost of electricity (*COE* [mill/kWh]) is the figure of merit for advanced tokamak power plants and serves as the ultimate optimization parameter in the ARIES systems study. In the present costing algorithm, this quantity is defined as

$$COE = \frac{c_{AC} + (c_{O\&M} + c_{SCR} + c_F) \cdot (1+y)^Y}{8760 \cdot P_E \cdot p_f} + c_{D\&D} \tag{50}$$

where c_{AC}, $c_{O\&M}$, c_{SCR} and c_F are the annual costs representing the annualized capital cost charge, operations and maintenance cost, scheduled component replacement cost and fuel cost, respectively [M$ 1992]; $y = 0.05$ year^{-1}[41] is the escalation rate; $Y = 6$ years [41] is the construction period; P_E is the net electric power [MW]; $p_f = 0.85$ [41] is the plant capacity factor; and $c_{D\&D}$ is the decontamination and decommissioning allowance in mills/kWeh. The escalation factor over the construction period increases the estimated cost of these cost elements from the beginning of construction to the commencement of power production.

The annual capital cost charge is evaluated as

$$c_{AC} = FCR \cdot c_{99} \tag{51}$$

where $FCR = 0.0965$ is the fixed charge rate [40,41] and c_{99} is the total capital cost. The fixed charge rate is based on the cost of money, federal tax rates, depreciation rates, salvage value, and construction period.

The annual operations and maintenance cost is given as

$$c_{O\&M} = 74.4 \cdot \left(\frac{P_E}{1200}\right)^{0.5} \cdot \xi_{O\&M}(LSA) \tag{52}$$

where $\xi_{O\&M}(LSA)$ is the cost credit factor that corresponds to the given level of safety assurance, as shown in Table 10.

The annual scheduled component replacement cost sums up the expenses of replacing the plasma-facing components such as the first wall, blanket, reflector and the impurity control system every 3-4 years:

$$c_{SCR} = (c_{22.1.1} + c_{22.1.8}) \cdot CRF(X_0, L) \cdot F \cdot \frac{\left(1 + \xi_{96}(LSA)\right)}{L} \tag{53}$$

Table 13
Accounts 23 through 27.

Number	Account title	Cost [M$ 1992] Ref. ARIES-AT
23.0	Turbine plant equipment	$c_{23.0} = 243.34 \cdot \left(\frac{P_{ET}}{1{,}200}\right)^{0.83} \cdot \xi_{23.0}(LSA)$
23.1	Turbine generators	$c_{23.1} = 0$ (TBD)
23.2	Main steam system	$c_{23.2} = 0$ (TBD)
23.3	Heat rejection systems	$c_{23.3} = 0$ (TBD)
23.4	Condensing system	$c_{23.4} = 0$ (TBD)
23.5	Feed heating system	$c_{23.5} = 0$ (TBD)
23.6	Other turbine plant equipment	$c_{23.6} = 0$ (TBD)
23.7	Instrumentation and control	$c_{23.7} = 0$ (TBD)
24.0	Electric plant equipment	$c_{24.0} = 127.97 \cdot \left(\frac{P_{ET}}{1{,}200}\right)^{0.49} \cdot \xi_{24.0}(LSA)$
24.1	Switchgear	$c_{24.1} = 0$ (TBD)
24.2	Station service equipment	$c_{24.2} = 0$ (TBD)
24.3	Switchboards	$c_{24.3} = 0$ (TBD)
24.4	Protective equipment	$c_{24.4} = 0$ (TBD)
24.5	Electrical structures and wiring containers	$c_{24.5} = 0$ (TBD)
24.6	Power and control wiring	$c_{24.6} = 0$ (TBD)
24.7	Electrical lighting	$c_{24.7} = 0$ (TBD)
25.0	Miscellaneous plant equipment	$c_{25.0} = 61.21 \cdot \left(\frac{P_{ET}}{1{,}200}\right)^{0.59} \cdot \xi_{25.0}(LSA)$
25.1	Transportation and lifting equipment	$c_{25.1} = 0$ (TBD)
25.2	Air and water service systems	$c_{25.2} = 0$ (TBD)
25.3	Communications equipment	$c_{25.3} = 0$ (TBD)
25.4	Furnishings and fixtures	$c_{25.4} = 0$ (TBD)
26.0	Heat rejection system [a]	$c_{26.0} = 62.17 \cdot \left(\frac{P_{REJ}}{2{,}300}\right) \cdot \xi_{26.0}(LSA)$
26.1	Heat rejection system structures	$c_{26.1} = 0$ (TBD)
26.2	Heat rejection system mechanical equipment	$c_{26.2} = 0$ (TBD)
26.98	Spare parts allowance	$c_{26.98} = 0$ (TBD)
26.99	Contingency allowance	$c_{26.99} = 0$ (TBD)
27.0	Special materials	$c_{27.0} = \sum_{i=1}^{3} c_{27.i}$
27.1	Reactor LM coolant/breeder [b]	$c_{27.1} = (13.68 \cdot f_{6Li} + 4.29) \times 10^{-3} \cdot m_{LM} \cdot \xi_{27.1}(LSA)$
27.2	Other	$c_{27.2} = 0.44 \cdot \xi_{27.2}(LSA)$
27.3	Reactor building cover gas	$c_{27.3} = 0.22 \cdot \xi_{27.3}(LSA)$

[a] P_{REJ} is the rejected power [MW].
[b] m_{LM} is the mass of the liquid metal [tonne], $f_{6Li} = 0.9$ as recommended in [39].

In the Eq. (53), $c_{22.1.1}$ and $c_{22.1.8}$ are the costs calculated in the costing accounts that represent the contribution from the plasma-facing components (Table 12); *CRF* is the capital recovery factor; $X_0 = 0.0435$ [41] is the effective, tax-adjusted cost of money in constant dollars; L is the interval between the scheduled replacements of the plasma-facing components; $F = 1.272$ [41] is the present worth of the revenue requirements for a unit investment that is depreciated for tax purposes over a period of 5 years and $\xi_{96}(LSA)$ is the cost credit factor for the project contingency (account 96), given in Table 10. The interval between the scheduled replacements of the plasma-facing components is calculated as:

$$L = \frac{I_\omega \tau}{\hat{I}_\omega} \tag{54}$$

where the term $I_\omega \tau$ [MW year/m^2] is the neutron fluence life and $\hat{I}_\omega$ [MW/m^2] is the maximum neutron wall loading at the outboard mid-plane. The neutron fluence life for different blanket options used in the ARIES systems code is given in Table 7. For the given values of X_0 and L, the capital recovery factor is estimated by

$$CRF = \frac{X_0}{1 - (1 + X_0)^{-L}} \tag{55}$$

The annual fuel costs c_F and the decontamination and decommissioning allowance $c_{D\&D}$ are respectively estimated as

$$c_F = 0.03 \cdot \frac{8760 \cdot P_E \cdot p_f}{(1 + y)^Y} \tag{56}$$

$$c_{D\&D} = \xi_{D\&D}(LSA) \tag{57}$$

where $\xi_{D\&D}(LSA)$ is the cost credit factor given in Table 10.

8. Results and discussion

8.1. Validation of new ARIES systems code against ARIES-AT published data

The ARIES systems code was validated against the ARIES-AT baseline. The physics, engineering and costing parameters for this model are provided in Ref. [9]. The plasma parameters of the baseline model are duplicated by the physics module of the new ARIES systems code. The power core geometry was generated by using the existing CAD data for the ARIES-AT. Some modifications were made by updating the TF and PF magnets to more realistic models. In addition, the power flow was estimated with more attention to detail than in case of the ARIES-AT. The materials and other relevant engineering and costing information are obtained from the ARIES

program public database [1]. The level of safety assurance is equal to unity for the SiC system (i.e., LSA=1).

The direct costs of the ARIES-AT estimated by the ARIES systems code are compared to the baseline data in the bar chart given in Fig. 13. The cost outputs from different accounts are shown in 1992 dollars in order to match the original report. The numerical value of each cost output is provided next to the corresponding bar, while the relative departures of the costs obtained by the new systems code from those provided in Ref. [9] are shown in boldface (green font was used for positive departure, red for negative). The account 22. "Reactor plant equipment" has the most significant impact on the total direct cost and depends on the large number of parameters, including volumes and materials of all the power core elements, areas of the divertor plates, volume of the primary structure and the thermal power, as shown in Table 12. In this case, the ARIES systems code matches the baseline within 0.71%. The difference originates from the updated models of the TF and PF magnets as well as from the more accurate power flow algorithm. The updated power flow also has an impact on the cost outputs from the accounts 21 and 23 through 25 which are all functions of the gross electric power. In this case, the difference between the ARIES systems code output and the ARIES-AT baseline varies from as low as 1.98% (account 23. "Turbine Plant Equipment") to as high as 8.22% (account 25. "Miscellaneous Plant Equipment"). However, the account 25 with the cost output of 51.25 M$ has a relatively low impact on the total direct cost. The most significant mismatch of 12.39% between the new model and the reference is evident from the account 27. for "Special materials". The cost output of this account is a function of the mass of the liquid metal (PbLi), which is used as a coolant for the first wall, blanket, divertor and HT shield. The new ARIES systems code estimates the mass of the liquid metal by integration across the volumes of all of the aforementioned components while a different method/formula may have been used for the ARIES-AT. The outputs of the costing accounts 20 and 26 estimated by the new ARIES systems code match exactly the reference ARIES-AT. In case of the account 20, a simple numerical value is used as an output. The account 26 is a function of the rejected power, ($P_{REJ} = P_{ET} - P_{TH}$), where P_{ET} and P_{TH} are the gross electric and thermal power, respectively.

The indirect costs estimated by the ARIES systems code are compared to the ARIES-AT baseline in Fig. 14. The total direct cost is the output of the account 90. The difference of 1.11% between the new model and the reference is accrued by adding the outputs from the direct costing accounts 20–27. Since the costing accounts 91–99 are all directly proportional to the account 90, as shown in Section 6.2, the relative difference between the new systems code prediction and the published ARIES-AT data remains the same throughout the indirect costing accounts.

The cost of electricity and the comprising costs normalized by the net electric power output are compared in Table 14. The most significant component is the capital return, which is directly proportional to the total capital cost given in the account 99. The relative difference of 1.11% between the prediction of the ARIES systems code and the baseline data carries over from the comparison of the indirect costs. The remaining costs, including the operations and maintenance cost ($c_{O\&M}$), component replacement cost (c_{SCR}), fuel replacement cost (c_F) and decontamination and decommissioning allowance ($c_{D\&D}$) are identical. As a result, the cost of electricity, which is the sum of the aforementioned accounts differs between the new model and the reference ARIES-AT by 0.86%.

8.2. Utilization of new ARIES systems code for production and analysis of large databases of advanced tokamaks

A large database of tokamak power plant models was generated in order to demonstrate the capability of the ARIES systems code to visualize and extract meaningful information from a dense "cloud" of operating points that are spread over an arbitrary parametric design space. This database was initiated by scanning the plasma parameters within desired limits, as shown in Table 15. The purpose of this scan was to generate a large set of tokamaks that span the range from ARIES-I to ARIES-AT of the parametric space and thus provide an insight into the key parameters and trends that affect the cost of electricity (*COE*). In Table 15, the differences between the adjacent numerical values of each scanned parameter (increments, as shown in the rightmost column) were successively reduced to their present values in order to capture the gradients of the significant parameters within the designated windows.

Table 16 illustrates the selective computational process which lead into a reduction in number of the acceptable plasmas/tokamaks with the net electric output of 1000 MW. The initial scan of the physics parameters was used as an input to the plasma physics module of the systems algorithm, which generated 16,380,000 different plasmas. These plasmas were subjected to the physics filters given in the Eq. (16) and thus, their number was reduced to 2,080,125 viable plasmas available for further processing. Engineering module of the systems code was used in order to build the remainder of the power plant model for each of these plasmas, including the power core and the power flow estimation. At this stage, the engineering filters given in the Eqs. (40)–(43) were applied, resulting in a number of surviving design points that was strongly dependent on the limit to peak heat flux on divertor $Q_{div\,lim}$ and varies from 2337 for $Q_{div\,lim} = 5\,\mathrm{MW/m^2}$ to 6811 for $Q_{div\,lim} = 12\,\mathrm{MW/m^2}$. The surviving design points were subjected to costing algorithms in order to estimate the cost of electricity. On a single Intel Core™ 2 Quad processor [42], the total processing time

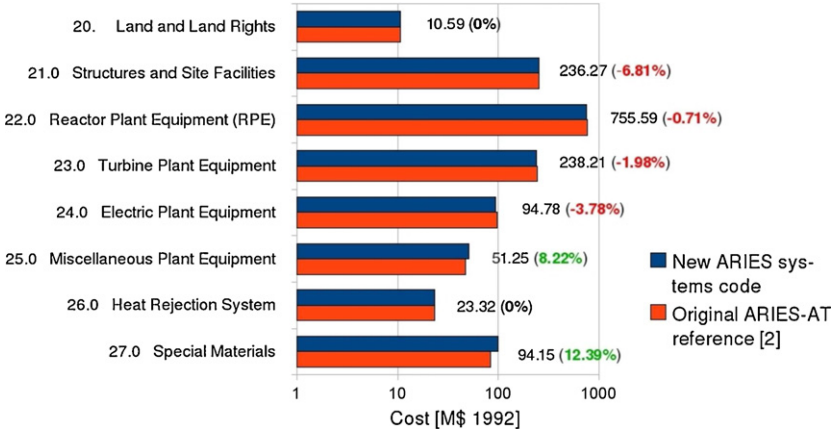

Fig. 13. Direct costs of ARIES-AT reference [9] estimated by the new ARIES systems code versus published data.

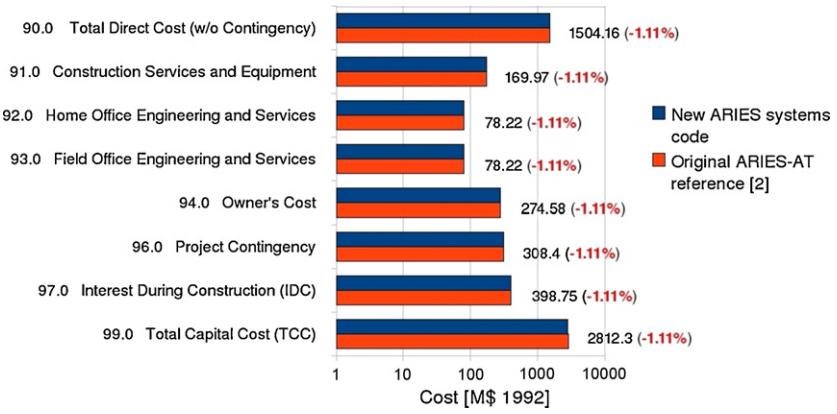

Fig. 14. Comparison between indirect costs of ARIES-AT estimated by the new ARIES systems code and published data.

Table 14
Cost of electricity (in 1992 $) and component costs for the ARIES-AT reference estimated by the new ARIES systems code versus published data [9].

Cost normalized by net electric power output	New ARIES systems code [mill/kWh]	ARIES-AT reference [9] [mill/kWh]	Relative difference [%]
Capital return $c_{AC}/(8760P_E p_f)$	36.46	36.87	1.11
Operations and maintenance $c_{O\&M}(1+y)^Y/(8760P_E p_f)$	6.87	6.87	0.00
Component replacement $c_{SCR}(1+y)^Y/(8760P_E p_f)$	3.51	3.51	0.00
Fuel cost $c_F(1+y)^Y/(8760P_E p_f)$	0.03	0.03	0.00
Decontamination and decommissioning allowance $c_{D\&D}$, Eq. (57)	0.25	0.25	0.00
Cost of electricity *COE*, Eq. (50)	47.12	47.53	0.86

Table 15
Scan of physics parameters used for generating the ARIES-DB-SiCLL database.

Parameter	Initial value	Final value	Increment
Toroidal field at plasma maj. radius B_T [T]	5.0	8.0	0.5
Plasma aspect ratio $a_{sp} = R/a$ [–]	4.0	4.0	0.0
Normalized beta β_N [–]	3.0	6.0	0.25
Cylindrical safety factor q_{cyl} [–]	−3.2	−4.6	0.2
Triangularity at 95% surface δ [–]	0.6	0.8	0.2
Density profile exponent a_n [–]	0.472	0.472	0.0
Temperature profile exponent a_t [–]	0.964	0.964	0.0
Auxiliary power P_{aux} [MW]	37.0	37.0	0.0
Fraction of Greenwald density $f_{Gw} = n/n_{Gw}$ [–]	0.4	1.1	0.05
Ratio of fusion to auxiliary power $Q = P_{fus}/P_{aux}$ [–]	20.0	40.0	5.0
Plasma elongation κ [–]	1.8	2.2	0.2
Flattop time t_{flati} [s]	1000.0	1000.0	0.0
Flux swing required from central solenoid d_{fcs} [MW/m^2]	300.0	300.0	0.0
Ratio of effective particle confinement time to energy confinement time $t_{\text{pote}} = \tau_p^*/\tau_E$ [–]	10.0	10.0	0.0
Plasma internal self-inductance a_{li} [H]	0.5	0.5	0.0
Ejima coefficient for resistive flux consumption c_e [–]	0.5	0.5	0.0
Breakdown flux $q_{brkdown}$ [MW/m^2]	10.0	10.0	0.0
Plasma major radius R [–]	4.5	9.0	0.5
Current drive efficiency η_{CD} [–]	0.3	0.3	0.0
Argon impurity fraction f_{imp} [–]	0.001	0.004	0.001
Charge of impurity Z_{imp} [–]	18.0	18.0	0.0
Ratio of plasma density at center to edge d_{rat} [–]	0.27	0.27	0.0

Table 16
Number of plasma operating points at different stages of computation.

Operation applied		Resulting number of plasmas
Scan of physics parameters		16,380,000
Rejection of non-valid plasma points		2,080,125
Engineering filters	$Q_{div\,lim} = 12$ MW/m^2	6811
	$Q_{div\,lim} = 8$ MW/m^2	5052
	$Q_{div\,lim} = 5$ MW/m^2	2337

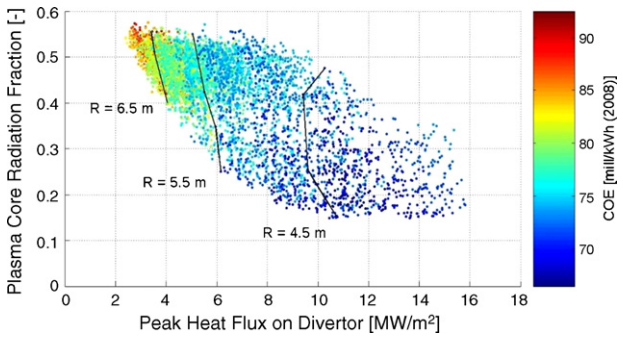

Fig. 15. Distribution of tokamak operating points in the parametric space defined by the peak heat flux on divertor and plasma core radiation fraction. Cost of electricity of each power plant is color-coded. Contour lines correspond to plasma major radius.

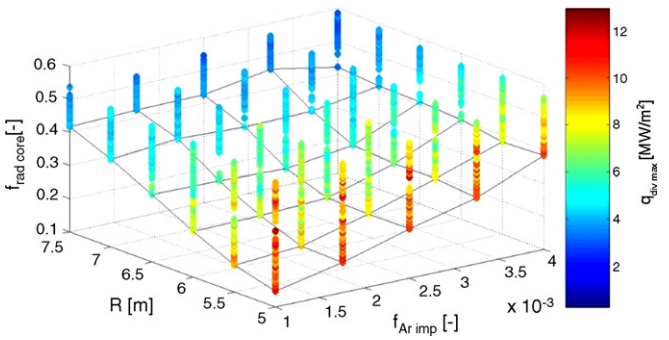

Fig. 16. Plasma core radiation fraction and peak heat flux on divertor (color-coded) as functions of argon impurity fraction and plasma major radius.

per each plasma by the physics module of the algorithm was 0.068 s, while the engineering and costing took 3.418 s per design point. By using four aforementioned processors equally loaded in a parallel mode, the total computational time was 653 h or approximately 27 days.

Fig. 15 depicts a relationship between the peak heat flux on divertor, plasma core radiation fraction, plasma major radius and cost of electricity over a range of major plasma radii. Plasma core radiation fraction is the ratio between the total radiated power from the plasma core and the sum of the powers that provide heat to the plasma,

$$f_{rad\,core} = \frac{P_{brem} + P_{cycl} + P_{line}}{P_{\alpha} + P_{aux}} \tag{58}$$

where P_{brem}, P_{cycl} and P_{line} are the Bremsstrahlung, cyclotron and line radiation losses, respectively, P_{α} is the power of the alpha particles and P_{aux} is the auxiliary heating power supplied to the plasma. Each data point in Fig. 15 represents a different tokamak power plant with the corresponding peak heat flux on divertor and plasma core radiation fraction shown as coordinates in 2D Cartesian system of reference. The contour lines connect the tokamaks with the same plasma major radii while the *COE* corresponding to each plant is color coded, as defined by the numerical scaling on the side-bar. The graph reveals the expected direct proportionality between the *COE* and the plasma major radius, which is rooted in the fact that the size of the power core scales with the plasma major radius and determines the direct costs. The distribution of data points shows that the range of plasma core radiation fractions gains in magnitude by increasing the plasma major radius while the opposite trend can be observed for the peak heat flux on divertor. Both trends are consistent with the observation that the magnitudes of the plasma heating power $P_{\alpha} + P_{aux}$ decrease with the plasma major radius while the total radiation from the plasma core increases. At $R = 4.5$ m, the plasma heating power (alpha power + auxiliary power) spans from 410 to 570 MW, while at $R = 7.5$ m, this range is from 400 to 500 MW. At the same time, the sum of radiation losses $P_{brem} + P_{cycl} + P_{line}$ is within 73–225 MW at the lowest plasma major radius and reaches 200–280 MW at the highest. A realistic, material driven limit to the peak heat flux on divertor is considered to be between 5 and 8 MW/m^2, which places the region of possibly attractive tokamaks at the section of the graph between $R = 5$ m and $R = 6$ m.

Plasma impurities in form of noble gases are typically used in order to enhance the radiation from the plasma core, which in return reduces the heat load on divertor and increases the availability of smaller and less expensive tokamaks. In the present tokamak model, the argon impurity fraction was varied from 0.001 to 0.004, with an increment of 0.001, as shown in Table 15. The upper value is set by the limitations of the current drive model used in the present algorithm. Fig. 16 shows the dependence of the plasma core radiation fraction on the argon impurity fraction and the plasma major radius. It is evident that the argon impurities have a strong impact on increasing the radiation from the plasma core at small values of R, while this effect diminishes at large plasma major radii. As shown in Fig. 16, peak heat flux on divertor (color-coded) complements the core radiation fraction and can clearly be alleviated by adding Ar impurities. At $R = 5$ m, the peak heat flux on divertor varies from 7.8 MW/m^2 to 13.0 MW/m^2 when the Ar impurity fraction is set to 0.001. At the same plasma major radius, the peak heat flux on divertor drops to 6.55–10.83 MW/m^2 when the Ar impurity fraction is increased to 0.004.

Fig. 17 shows the dependence between the volume average electron density, volume average electron temperature, limiting heat flux on divertor and cost of electricity. The data visualization style is similar to the graph depicted in Fig. 15, except that the plasma physics parameters are represented in form of 2D coordinates of each data point and the limiting heat flux on divertor is represented by contours. Based on the *COE* distribution, the cost-efficiency of the plasma increases with the volume average electron density, which is the expected result and can be explained by the fact that tokamaks with smaller, less expensive power cores need higher density plasmas in order to yield the same net electric power as their larger counterparts. The plasmas with high volume average temperatures of 30–35 keV congregate in the region of low density plasmas where high values of *COE* and low values of peak heat flux on divertor imply the large plasma major radii. These high temperatures can explain the increase of core radiation fraction with the plasma major radius, as described earlier. The region of possibly attractive plasmas can be found between the contour lines of the limiting heat flux on divertor between 5 MW/m^2 and 8 MW/m^2.

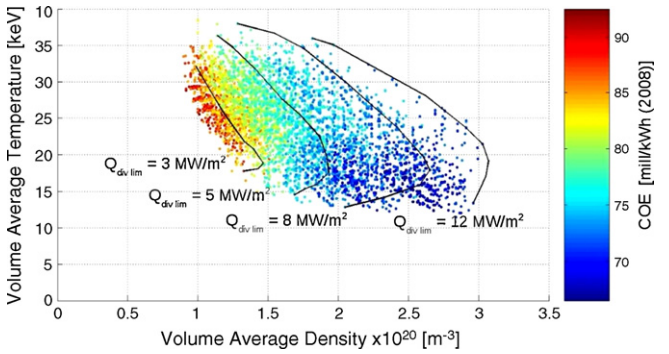

Fig. 17. Distribution of tokamak operating points in the parametric space of volume average electron density and volume average electron temperature. Cost of electricity corresponding to each power plant is color-coded. Contour lines represent the limiting heat flux on divertor.

An additional snapshot of the database is provided by plotting the distribution of the *COE* values across the 2D parametric space that consists of the plasma major radius R and the toroidal magnetic field at plasma major radius B_T, as shown in Fig. 18. At each (R,B_T) location the *COE* varies by 5–8%, depending on the values of other parameters. The net electric power throughout the tokamak database is within ±0.5% from its nominal value of 1000 MW, which does not account for this local variation in *COE*. However, the power cycle efficiency spans between 0.5 and 0.59, depending on the peak neutron wall load and the peak heat flux on the first wall, as discussed in Section 5.2. This allows for the existence of plasmas with a range of different fusion powers that yield the same net electric power at fixed R and B_T. For example, at $R = 5$ m and $B_T = 5.5$ T, the fusion power varies from 1825 to 2210 MW. At this location, several different quantities cause variations in direct costs and therefore the COE:

- Gross electric power P_{ET}~1160–1316 MW affects the account 21. "Structures and site facilities", shown in Table 11, and the accounts 23-26 shown in Table 13.
- Average neutron wall load q_{nwl}~2.46–2.95 MW/m^2 affects the HT shield thickness and therefore its volume and cost, included as a sub-account 22.1.2 of the account 22. "Reactor plant equipment", as shown in Table 12.
- Thermal power P_{TH}~2020–2505 MW affects the accounts 22.2 "Main heat transfer system" and 22.6 "Other reactor plant equipment", as evident from Table 12.

In Fig. 18, the minimum values of the *COE* at each (R, B_T) location are connected into an optimal surface by a 2nd order interpolation. As anticipated, the optimal *COE* descends with reduction of the machine size (~R) and TF magnet strength (B_T) and reaches the overall minimum of 67.98 mill/kWh (2008 dollars) at $R = 5$ m and $B_T = 5$ T. The ARIES-AT, shown for comparison as a single data point, is reasonably close to the optimal surface with a *COE* of 71.96 mill/kWh, plasma major radius of 5.2 m and the corresponding toroidal magnetic field of 5.86 T.

In Fig. 18, the ratio between the line-averaged electron density and the Greenwald density limit $n_e/n_{Gwld\,lim}$ is depicted by color coding each individual data point based on the numerical value of this parameter. In addition, the values of the $n_e/n_{Gwld\ \mathrm{lim}}$ corresponding to the tokamaks that lie on the optimal *COE* surface are interpolated and projected onto this surface using the same numerical color mapping as for the individual data points. The Greenwald density ratio for the entire database varies from 0.6 to 1.1. For the tokamaks on the optimal *COE* surface, the line-averaged electron density varies between 10% below and 10%percent above the Greenwald limit. At the same time, the plasmas with the highest *COE* at each (R, B_T) location have the lowest Greenwald density ratio

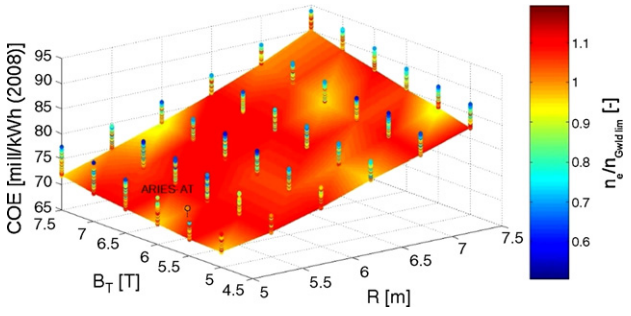

Fig. 18. Cost of electricity *COE* as a function of plasma major radius R, toroidal magnetic field at plasma major radius B_T and Greenwald density ratio $n_e/n_{Gwldlim}$, color-coded. ARIES-AT data point is provided for comparison.

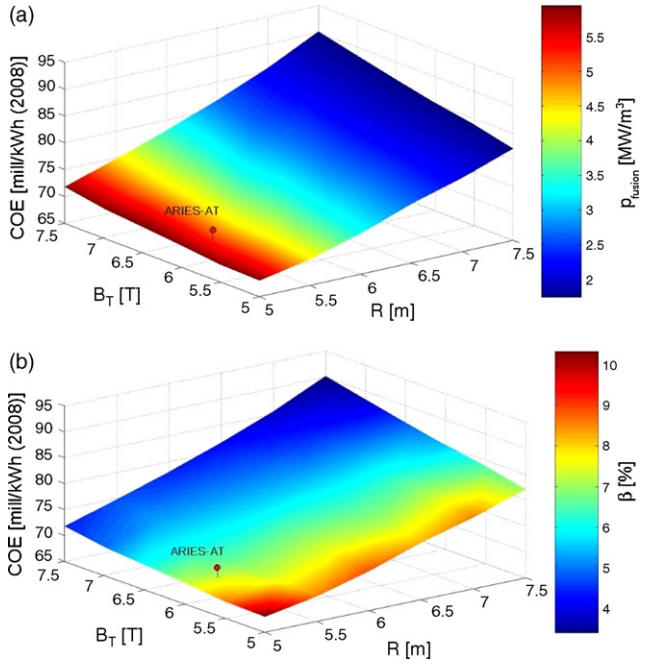

Fig. 19. Distribution of fusion power density (part **a**) and toroidal beta (part **b**) across the most cost-effective tokamaks with different plasma major radii and corresponding toroidal magnetic fields.

of 0.6. This confirms the well established knowledge that highly efficient plasmas are those close to their density limits [43]. For comparison, the ARIES-AT plasma has the electron line density of 2.423×10^{20} m^{-3}, while the Greenwald density limit for this case is 2.414×10^{20} m^{-3}. The data in Fig. 18 also suggests that Greenwald density ratio is insensitive to either the plasma major radius or the toroidal field at plasma major radius.

In Fig. 19, the distribution of fusion power density (p_{fusion}, part **a**) and toroidal beta (β, part **b**) across the set of tokamaks with the optimal *COE* is depicted in the parametric space of R and B_T. The fusion power density (p_{fusion}~$\beta^2 B_T^4$) is constant along the toroidal magnetic field and uniformly drops by a factor of 3 with the plasma major radius. As a consequence, the magnitude of β increases sharply with reduction in the magnet strength and moderately with reduction in the machine size, peaking at 10.39% ($R = 5$ m, $B_T = 5$ T). For a comparison, the ARIES-AT has a toroidal beta of 9.18. The ARIES-AT study [9] suggested that high values of β allow for the utilization of a high bootstrap current fraction, which as a payoff allows a steady state confinement with lower toroidal magnetic fields. For the tokamak with the peak β and the lowest overall *COE*, the bootstrap current fraction is as high as 0.98, while the ARIES-AT value is 0.91. The most cost-efficient tokamak with the same plasma major radius and a toroidal magnetic field of 7.5 T has the bootstrap current fraction of 0.86.

Table 17 provides a list of the most relevant physics and engineering parameters for five tokamaks with the lowest *COE*. Even though the variation in *COE* across these tokamaks is relatively small (approximately 1% or 0.66 mill/kWh in 2008 dollars), the variation of normalized beta is between 4.8 and 6.0, which is quite significant and allows some flexibility in selection of the optimal design. The ARIES-AT, for instance, features a normalized beta of 5.45, a value that is about 10% below the Troyon limit. A similar observation can be made for the Greenwald density ratio, which varies between 0.95 and 1.1. All of the tokamak designs shown in Table 17, have values of the heat flux on divertor that are in close proximity of the present limit of 8 MW/m^2.

Table 17
Most relevant physics and engineering parameters for five selected tokamak designs with lowest cost of electricity. Heat flux to divertor is limited to 8 MW/m^2.

Parameter	Value				
Cost of electricity, *COE* [mill/kWh (2008)]	66.84	66.91	66.94	67.00	67.48
Plasma major radius, R [m]	5.0	5.0	5.0	5.0	5.0
Toroidal magnetic field at plasma major radius, B_T [T]	5.0	5.0	5.0	5.0	5.5
Normalized beta, β_N [–]	5.8	5.5	6.0	5.3	4.8
Greenwald density fraction, $n/n_{Gwld\,lim}$ [–]	1.0	1.1	0.95	1.1	1.05
Plasma core radiation fraction, $f_{rad\,core}$ [–]	0.32	0.24	0.26	0.31	0.31
Peak heat flux on divertor, $q_{div\,max}$ [MW/m^2]	7.53	7.94	7.86	7.62	7.79
Peak radiated heat flux on the first wall, $q_{FW\,max}$ [MW/m^2]	0.36	0.30	0.31	0.36	0.37
Average neutron wall load, q_{nwl} [MW/m^2]	2.57	2.55	2.53	2.58	2.59
Plasma current, I_p [MA]	11.93	10.68	11.93	11.27	11.75
Plasma elongation, κ [–]	2.2	2.2	2.2	2.2	2.2
Safety factor at 95% surface, q_{95} [–]	3.4	3.8	3.4	3.6	3.8
Multiplier on energy confinement scaling, H_{98} [–]	1.75	1.63	1.85	1.55	1.53
Total auxiliary power into the plasma, P_{aux} [MW]	46.90	53.22	46.23	53.81	53.85
Bootstrap current fraction, f_{bs} [–]	0.925	0.989	0.965	0.894	0.854
Effective charge, Z_{eff} [–]	2.085	1.788	1.875	2.017	2.037

9. Conclusions

The ARIES systems code is being developed as a general purpose tool for parametric design space analysis and optimization of advanced tokamak models. As a foundation of the systems code, the custom-made toolbox of C++ classes and generic functions was built for a wide scope of possible applications in systems analysis of power plants. The algorithms presented in this paper, however, were developed for tokamaks that are similar in configuration to the ARIES-AT but allow for a variety of different options, such as plasma shape and size, blanket options, and type and size of the magnets. The parametric space approach assumed in this analysis derives information from a large database of viable tokamak systems instead of using a single optimal solution. This became possible due to ever-increasing ubiquity of inexpensive computing power, which allows for creation and storage of millions of power plant models on a desktop-type computer within days. A similar approach in the eighties would have required a Cray supercomputer and prohibitively expensive data processing/storage arrangements.

Test results presented in Section 8. benchmarked the new ARIES systems code against the ARIES-AT as a reference tokamak power plant and demonstrated several possible ways a rich database of models can be exploited. The "cloud" of operating points was visualized in 2D and 3D parametric spaces to reveal the key parameters that impact the cost of electricity and their mutual dependence. The visualization highlighted several well-understood effects, such as the proportionality of the *COE* to plasma major radius and toroidal field at plasma major radius, tradeoff between the plasma energy density and magnetic energy density (β versus B_T), impact of the argon impurities on the plasma core radiation fraction and peak heat flux on divertor and impact of the electron density on the *COE*. In addition to plotting multiple parameters across the "universe" of tokamaks, several operating points with the lowest *COE* were presented with the most relevant physics and engineering parameters. This was done in order to "zoom" into a narrower span of parameters likely to harbor the optimal machines. For these operating points, the magnitudes of the peak heat flux on divertor were close to a limit of 8 MW/m^2 which signals possible cost benefits from either shifting this constraint to higher values (by searching for more advanced divertor plate materials) or from alleviating the divertor heat flux through enhancing the radiation from the power core.

This introductory study lays out a path for an in-depth analysis of the operating parametric space of advanced tokamaks. A more detailed physics and engineering assessment will be complemented by a full optimization of the tokamak model and described in a subsequent publication. This assessment will also include a comparison of the cost impact of utilizing the two blanket configurations described in Section (the Pb–17Li+SiC$_f$/SiC and *DCLL* options). A complementary effort is being accomplished to document and update the ARIES cost data base and costing algorithms to be compatible with past study results and reflect the current cost databases and costing trends. There is a rich heritage of economic studies relating to conceptual fusion power plants, upon which the ARIES code is based, as evidenced in this paper. However, the assumptions upon which these estimates are based are now dated and may be obsolete and inconsistent. This costing update effort is meant to document the past efforts and offer new costing models consistent with the evolutionary physics and technology changes evidenced in the new fusion design concepts. These new costing models will be included in the new ARIES systems code to enable more consistent and viable performance and economic comparisons and trade studies.

Acknowledgement

This work was supported by the United States Department of Energy, Office of Fusion Energy DE-FC03-95ER54299.

References

[1] ARIES Program Public Information Site, Available from http://aries.ucsd.edu/ARIES.
[2] R.L. Miller, and the ARIES Team, The ARIES-I high field tokamak reactor: design point determination and parametric studies, Proceedings of the 13th Symposium on Fusion Engineering (IEEE, Knoxville, TN), 2, 1989, 1027.
[3] F. Najmabadi, the ARIES Team, The ARIES-AT advanced tokamak, advanced technology fusion power plant, Fusion Engineering and Design 80 (2006) 3.
[4] C.G. Bathke, A comparison of steady-state ARIES and pulsed PULSAR tokamak power plants, Fusion Technology 26 (1994) 1163.
[5] C.G. Bathke, R.L. Miller, Evolution of the ARIES-I design in the ARIES and PULSAR projects, pp. 1135–1138, Proceedings of 16th IEEE Symposium on Fusion Engineering, 1995.
[6] C.G. Bathke, Systems analysis in support of the selection of the ARIES-RS design point, Fusion Engineering and Design 38 (1997) 59–86.
[7] R.L. Miller, Systems context of the ARIES-AT conceptual fusion power plant, Fusion Technology 39 (2) (2001) 439.
[8] R.L. Miller, ARIES-ST design point selection, Fusion Engineering & Design 65 (2003) 199–213. SPPS study: R. Miller and The SPPS Team, The stellarator power plant study, University of California San Diego Report UCSD-ENG-004 (1997).
[9] C.E. Kessel, D. Meade, D.W. Swain, P. Titus, M.A. Ulrickson, Advanced tokamak plasmas in the fusion ignition research experiment, in: 20th IEEE/NPSS Symposium on Fusion Engineering, San Diego, 14–17 October, 2003.
[10] A.R. Raffray, L. El-Guebaly, S. Malang, I. Sviatoslavsky, M.S. Tillack, the ARIES Team, Advanced power core system for the ARIES-AT power plant, Fusion Engineering and Design 80 (2006) 79.
[11] L. El-Guebaly, P. Wilson, D. Henderson, M. Sawan, G. Sviatoslavsky, T. Tautges, R. Slaybaugh, B. Kiedrowski, A. Ibrahim, C. Martin, R. Raffray, S. Malang, J. Lyon, L.P. Ku, X. Wang, L. Bromberg, B. Merrill, L. Waganer, F. Najmabadi, the ARIES-CS Team, Designing ARIES-CS compact radial build and nuclear system: neutronics, shielding, and activation, Fusion Science and Technology 54 (3) (2008) 747–770.

[12] J. Lyon, L.P. Ku, L. El-Guebaly, L. Bromberg, L. Waganer, M. Zarnstorff, Team ARIES-CS, Systems studies and optimization of the ARIES-CS power plant, Fusion Science and Technology 54 (3) (2008) 694–724.
[13] F. Dahlgren, T. Brown, P. Heitzenroeder, L. Bromberg, the ARIES Team, ARIES-AT magnet systems, Fusion Engineering and Design 80 (2006) 139.
[14] S.C. Shulte, T.L. Willke, J.R. Young, Fusion reactor design studies: standard accounts for cost estimates, Pacific Northwest Laboratory, PNL-2648, 1978.
[15] C.C. Baker, M.A. Abdou et al., STARFIRE, a commercial tokamak fusion power plant study, Argonne National Laboratory report ANT/FPP-80–1, 1980.
[16] J.G. Delene, R.A. Krakowski, J. Shefield, R.A. Dory, GENEROMAK fusion physics, engineering and costing model, Oak Ridge National Laboratory Report, ORNL/TM-10728, 1988.
[17] J.P. Holdren, D.H. Berwald, R.J. Budnitz, J.G. Crocker, J.G. Delene, R.D. Endicott, M.S. Kazimi, R.A. Krakowski, B.G. Logan, K.R. Schultz, Report of the senior committee on environmental, safety, and economic aspects of magnetic fusion energy, Lawrence Livermore National Laboratory report UCRL-53766, 1989.
[18] C.G. Bathke, R.A. Krakowski, R.L. Miller, K.A. Werley, Chapter 2: systems studies of the ARIES-II and ARIES-IV tokamak fusion reactor study - the final report, UCLA report UCLA-PPG-1461, 1992.
[19] L. El-Guebaly, Nuclear performance assessment of ARIES-AT, Fusion Engineering and Design 80 (2006) 99–110.
[20] H.-S. Bosch, G.M. Hale, Improved formulas for fusion cross-sections and thermal reactivities, Nuclear Fusion 32 (1992) 611–631.
[21] D.E. Post, et al., Atomic data and nuclear data table 20 (1977) 397.
[22] F. Albajar, et al., Nuclear Fusion 41 (2001) 665.
[23] I. Fidone, et al., Nuclear Fusion 41 (2001) 1755.
[24] F. Albajar, et al., Electron cyclotron radiative heat transfer in fusion plasmas, unpublished.
[25] B.A. Trubnikov, M. Leontovich, in: Reviews of Plasma Physics, vol. 7, Plenum, New York, 1979, p345.
[26] ITER, Physics Expert Groups, Plasma confinement and transport, Nuclear Fusion 39 (1999) 2137.
[27] J.A. Snipes, et al., Plasma Physics and Controlled Fusion 42 (2000) A299.
[28] F. Ryter, et al., Plasma Physics and Controlled Fusion 44 (2002) A415.
[29] L. El-Guebaly, S. Malang, Toward the ultimate goal of tritium self-sufficiency: technical issues and requirements imposed on ARIES advanced fusion power plants, Fusion Engineering and Design 84 (2009) 2072–2083.
[30] L. El-Guebaly, Overview of ARIES-RS neutronics and radiation shielding: key issues and main conclusions, Fusion Engineering and Design 38 (1997) 139–158.
[31] L. El-Guebaly, the ARIES team, ARIES-ST nuclear analysis and shield design, Fusion engineering and Design 65 (2003) 263–284.
[32] A.R. Raffray, L. El-Guebaly, T. Ihli, S. Malang, X. Wang, the ARIES-CS Team, Engineering design and analysis of the ARIES-CS power plant, Fusion Science & Technology 54 (3) (October 2008) 725–746.
[33] W. Fundamenski, et al., Nuclear Fusion 44 (2004) 20.
[34] R. Miller and The SPPS Team, The stellarator power plant study, University of California San Diego Report UCSD-ENG-004, 1997.
[35] J.P. Holdren, D.H. Berwald, R.J. Budnitz, J.G. Crocker, J.G. Delene, R.D. Endicott, M.S. Kazimi, R.A. Krakowski, B.G. Logan, K.R. Schultz, Report of the senior committee on environmental, safety, and economic aspects of magnetic fusion energy, Lawrence Livermore National Laboratory report UCRL-53766 (1989).
[36] J.P. Holdren, D.H. Berwald, R.J. Budnitz, J.G. Crocker, J.G. Delene, R.D. Endicott, M.S. Kazimi, R.A. Krakowski, B.G. Logan, K.R. Schultz, Exploring the competitive potential of magnetic fusion energy: the interaction of economics with safety and environmental characteristics, Fusion Technology 13 (1988) 7.
[37] J.G. Delene, K.A. Williams, B.H. Shapiro, Nuclear energy cost data base, US DOE report DOE/NE-0095, September 1988.
[38] R.L. Miller, ARIES Systems code (ASC) cost database update, informal memo, April 13, 2008.
[39] B. Badger, I.N. Sviatoslavsky, S.W. Van Sciver, G.L. Kulcinski, G.A. Emmert, D.T. Anderson, et al., UWTOR-M: A conceptual modular stellarator power reactor, University of Wisconsin report UWFDM-550, October 1982.
[40] J.G. Delene, R.A. Krakowski, J. Sheffield, R.A. Dory, GENEROMAK fusion physics, engineering, and costing model, Oak Ridge National Laboratory report ORNL/TM-10728, June 1988.
[41] U.S. Department of Energy, Office of Nuclear Energy, Nuclear energy cost data base, a reference data base for nuclear and coal-fired power plant power generation cost analysis, USDOE report DOE/NE-0096 (September 1988).
[42] Intel Public Information Site on Core^2 Quad Processor, available from http://www.intel.com/products/processor/core2quad/index.htm.
[43] M. Greenwald, J. Terry, S. Wolfe, S. Ejima, M. Bell, S. Kaye, G.H. Neilsen, A new look at density limits, Nuclear Fusion 28 (1988) 2199.